
Fractal Autoencoders for Feature Selection

Xinxing Wu
University of Kentucky
Lexington, Kentucky, United States

Qiang Cheng*
University of Kentucky
Lexington, Kentucky, United States

October 20, 2020

ABSTRACT

Feature selection reduces the dimensionality of data by identifying a subset of the most informative features. In this paper, we propose an innovative framework for unsupervised feature selection, called fractal autoencoders (FAE). It trains a neural network (NN) to pinpoint informative features for global exploring of representability and for local excavating of diversity. Architecturally, FAE extends autoencoders by adding a one-to-one scoring layer and a small sub-NN for feature selection in an unsupervised fashion. With such a concise architecture, FAE achieves state-of-the-art performances; extensive experimental results on fourteen datasets, including very high-dimensional data, have demonstrated the superiority of FAE over existing contemporary methods for unsupervised feature selection. In particular, FAE exhibits substantial advantages on gene expression data exploration, reducing measurement cost by about 15% over the widely used L1000 landmark genes. Further, we show that the FAE framework is easily extensible with an application.

1 Introduction

High-dimensional data is pervasive in almost every area of modern data science [Clarke et al., 2008, Blum et al., 2020]. Dealing with high-dimensional data is challenging due to the known phenomenon – the curse of dimensionality [Bellman, 1957]. In numerous applications, principal component analysis (PCA) [Pearson, 1901] and autoencoders (AE) [Rumelhart et al., 1985, Ballard, 1987], two traditional and simple approaches, are typically used for dimensionality reduction. For example, PCA is adopted to reduce the dimensions of gene expression data before the extraction of the samples’ rhythmic structures [Anafi et al., 2017]; autoencoders are employed to process high-dimensional datasets prior to clustering [Xie et al., 2016] and subspace learning [Ji et al., 2017]. Despite their widespread usage, the interpretation of lower-dimensional feature spaces produced by PCA and AE is not straightforward, because these feature spaces are different from the original feature space. In contrast to PCA and AE, feature selection allows for ready interpretability with the input features, by identifying and retaining a subset of important features directly from the original feature space [Guyon and Elisseeff, 2003].

There exist various feature selection approaches. According to whether labels are used, they can be categorized as supervised, semi-supervised, and unsupervised methods [Alelyani et al., 2013]. Unsupervised approaches have potentially extensive applications, since they do not require labels that can be rare or expensive to obtain. A variety of techniques for unsupervised feature selection have been proposed, e.g., Laplacian score (LS) [He et al., 2005] and concrete autoencoders (CAE) [Abid et al., 2019]. While often used, the existing approaches may still exhibit suboptimal performance in downstream learning tasks on many datasets, which can be seen, e.g., in Table 3. There are two major reasons that cause such under-performance. First, the space to search for potentially important subsets of features in the absence of the guidance by labels is often very large, which renders unsupervised feature selection to be like finding a needle in a haystack. Second, it is necessary, yet challenging, to take account of the inter-feature interactions. Ideally, the selected features should be globally representative and as diverse as possible. If the selected features are all important yet highly correlated, they may be capable of representing only partial data, and thus they would hardly comprise a globally representative feature subset. For example, if a pixel of a natural image is important, then some neighboring ones are also likely to be so because of the typical spatial dependence in images; thus, to select diverse, salient features to represent the overall contents, if a pixel is important and selected, those neighboring pixels of high correlations with it should not be included into the feature subset. Existing unsupervised approaches have limited

*qiang.cheng@uky.edu.

abilities to simultaneously explore the large search space for features that can represent the overall contents and take into account the diversity, which is reflected by the inter-correlation, of features, thus leading to suboptimal performances.

To overcome these difficulties, in this paper we propose a novel unsupervised feature selection framework, called fractal autoencoders (FAE). It trains a neural network (NN) to identify potentially informative features for representing the contents globally; simultaneously, it exploits a dependence sub-NN to select a subset locally from the globally informative features to examine their diversity, which is efficiently measured by their abilities to reconstruct the original data. In this way, the sub-NN enables FAE to effectively screen out the highly correlated features; the global AE component of FAE turns out to play a crucial role of regularization to stabilize the feature selecting process, aside from its standard role of feature extraction. With our new architecture, FAE merges feature selection and feature extraction into one model, facilitating the identification of a subset of the most representative and diverse input features. To illustrate the extensive ability of the FAE framework, we use it to derive an h -Hierarchy FAE (h -HFAE) application to identify multiple subsets of important features.

In summary, our main contributions include:

- We propose a novel framework, FAE, for feature selection to meet the challenges of existing methods. It combines global exploration of representative features and local excavation of their diversity, thereby enhancing the generalization of the selected feature subset and accounting for inter-feature correlations.
- As our framework can be readily applicable or extensible to other tasks, we show an application to identify multiple hierarchical subsets of salient features simultaneously. More applications are also presented in the Supplementary Material.
- We validate FAE with extensive experiments on fourteen real datasets. Although simple, it demonstrates state-of-the-art performance for reconstruction on most of the benchmarking datasets. It also yields superior performance in a downstream learning task of classification. As a biological application, FAE reduces gene expression measurements by about 15% compared with L1000 landmark genes. Further, FAE exhibits more stable performance on varying numbers of selected features than contemporary methods.

The notations and definitions are given as follows. Let n , m , and k be the numbers of samples, features, and reduced dimensions, respectively. Let $\mathbf{X} \in \mathbb{R}^{n \times m}$ be a matrix containing the input data. A bold capital letter such as \mathbf{W} denotes a matrix; a lowercase bold capital letter such as \mathbf{w} denotes a vector; $\text{Diag}(\mathbf{w})$ represents a diagonal matrix with the diagonal \mathbf{w} ; \mathbf{w}^{\max_k} is an operation to keep the k largest entries of \mathbf{w} while making other entries 0, and $\mathbf{1}(\mathbf{w}^{\max_k})$ is a further operation to replace nonzero elements of \mathbf{w}^{\max_k} with 1. $\|\cdot\|_{\text{F}}$ denotes the Frobenius norm. $\text{Pos}(\mathbf{W})$ counts the number of positive values in \mathbf{W} .

The remaining of the paper is organized as follows. We first discuss the related work, then present our proposed approach, followed by extensive experiments. Finally, we apply FAE to identify multiple subsets of informative features.

2 Related Work

A variety of feature selection approaches have been proposed. They are usually classified into four categories [Alelyani et al., 2013, Li et al., 2017]: filter methods, which are independent of learning models; wrapper methods, which rely on learning models for selection criteria; embedder approaches, which embed the feature selection into learning models to also achieve model fitting simultaneously; hybrid approaches, which are a combination of more than one of above three. Alternatively, the approaches are categorized as supervised, semi-supervised, and unsupervised methods according to whether label information is utilized. Unsupervised feature selection has potentially broad applications because it requires no label information; yet, it is also arguably more challenging due to the lack of labels to guide the identification of relevant features. In this paper, we focus on unsupervised feature selection and briefly review typical methods below.

LS [He et al., 2005] is a filter method that uses the nearest neighbor graph to model the local geometric structures of the data. By selecting the features which are locally the smoothest on the graph, LS focuses on the local property yet neglects the global structure. SPEC [Zhao and Liu, 2007] is also a filter method based on general similarity matrix. It employs the spectrum of the graph to measure feature relevance and unifies supervised and unsupervised feature selection. Principal feature analysis (PFA) [Lu et al., 2007] utilizes the structure of the principal components of a set of features to select the subset of relevant features. It can be regarded as a wrapper method to optimize the PC coefficients, and it mainly focuses on globality. Multi-cluster feature selection (MCFS) [Cai et al., 2010] selects a subset of features to cover the multi-cluster structure of the data, where spectral analysis is used to find the inter-relationship between different features. Unsupervised discriminative feature selection (UDFS) [Yang et al., 2011] incorporates the discriminative analysis and $\ell_{2,1}$ regularization to identify the most useful features. Nonnegative discriminative feature selection (NDFS) [Li et al., 2012] jointly learns the cluster labels and feature selection matrix to select discriminative

features. It uses a nonnegative constraint on the class indicator to learn cluster labels and adopts an $\ell_{2,1}$ constraint to reduce the redundant or noisy features.

Recently, a few AE-based feature selection methods have been developed. Autoencoder feature selector (AEFS) [Han et al., 2018] combines autoencoders regression and $\ell_{2,1}$ regularization on the weights of the encoder to obtain a subset of useful features. It exploits both linear and nonlinear information in the features. Agnostic feature selection (AgnoS) [Doquet and Sebag, 2019] adopts AE with explicit objective function regularizations, such as the $\ell_{2,1}$ norm on the weights of the first layer of AE (AgnoS-W), $\ell_{2,1}$ norm on the gradient of the encoder (AgnoS-G), and ℓ_1 norm on the slack variables that constitute the first layer of AE (AgnoS-S), to implement feature selection. AgnoS-S is the best of the three, so in this study we will compare our approach with AgnoS-S. CAE [Abid et al., 2019] replaces the first hidden layer of AE with a “concrete selector” layer, which is the relaxation of a discrete distribution called concrete distribution [Maddison et al., 2017], and then it picks the features with an extremely high probability of connecting to the nodes of the concrete selection layer. The parameters of this layer are estimated by the reparametrization trick [Kingma and Welling, 2014]. CAE reports superior performance over other competing methods.

MCFS, UDFS, NDFS, AEFS, AgnoS, and CAE can be all regarded as embedded approaches. Though our proposed FAE model also embeds the feature selection into AE, which looks similar to AgnoS, AEFS, and CAE, it essentially differs from these existing methods: AEFS and AgnoS mainly depend on exploiting sparsity norm regularizations such as $\ell_{2,1}$ and ℓ_1 on the weights of AE to select features, which do not consider diversity; in contrast, FAE innovatively adopts a sub-NN to explicitly impose the desired diversity requirement on informative features. CAE adopts a probability distribution on the first layer of AE and selects features by their parameters. However, several neurons in the concrete selector layer may potentially select the same or redundant features, and the training requires that the average of the maximum probability of connecting to these neurons in the concrete selection layer exceed a pre-specified threshold of close to 1, which may be hard to attain for high-dimensional datasets; meanwhile, the second and third top features at different nodes of the concrete selector layer may be insignificant because of their trivial average probability. These potential drawbacks can limit the performance of CAE. In contrast, our proposed FAE does not depend on any probability distribution; rather, its sub-NN, with the guidance by the global-NN, directly pinpoints a subset of selected features, which makes FAE concise in architecture and easily applicable to different tasks.

3 Proposed Approach

In this section, we will present the architecture and formulation of FAE.

3.1 Overview of Our Approach

The architecture of our FAE approach is depicted in Figure 1. It enlists the AE architecture as a basic building block; yet, its structure is particularly tailored to feature selection. In the following, we will explain the architecture and its components in detail.

3.2 Formalization of Autoencoders

For AE, we formalize it as follows:

$$\min_{f,g} \|\mathbf{X} - f(g(\mathbf{X}))\|_{\mathbb{F}}^2, \quad (1)$$

where g is an encoder, and f is a decoder. $g(\mathbf{X})$ embeds the input data into a latent space $\mathbb{R}^{m \times k}$, where k denotes the dimension of the bottleneck layer of AE. Taking MNIST as an example, for $k = 49$, we visualize the encoded samples in Figure 2 (b). After being transformed, either nonlinearly or linearly, from the original space, the contents of each sample are not visually meaningful in the latent space.

3.3 Formalization of Unsupervised Feature Selection

Feature selection is to identify a subset of informative features in the original feature space, and it can be formalized as follows:

$$\min_{S^k, H} \|H(\mathbf{X}_{S^k}) - \mathbf{X}\|_{\mathbb{F}}^2, \quad (2)$$

where S^k denotes the subset of k features, \mathbf{X}_{S^k} is the derived data set from \mathbf{X} based on S^k , and H denotes a mapping from the space spanned by \mathbf{X}_{S^k} to $\mathbb{R}^{n \times m}$ in the absence of information about labels. The optimization problem in (2) is NP-hard [Natarajan, 1995, Hamo and Markovitch, 2005]. This paper will develop an effective algorithm to approximate the solution of (2) for unsupervised feature selection.

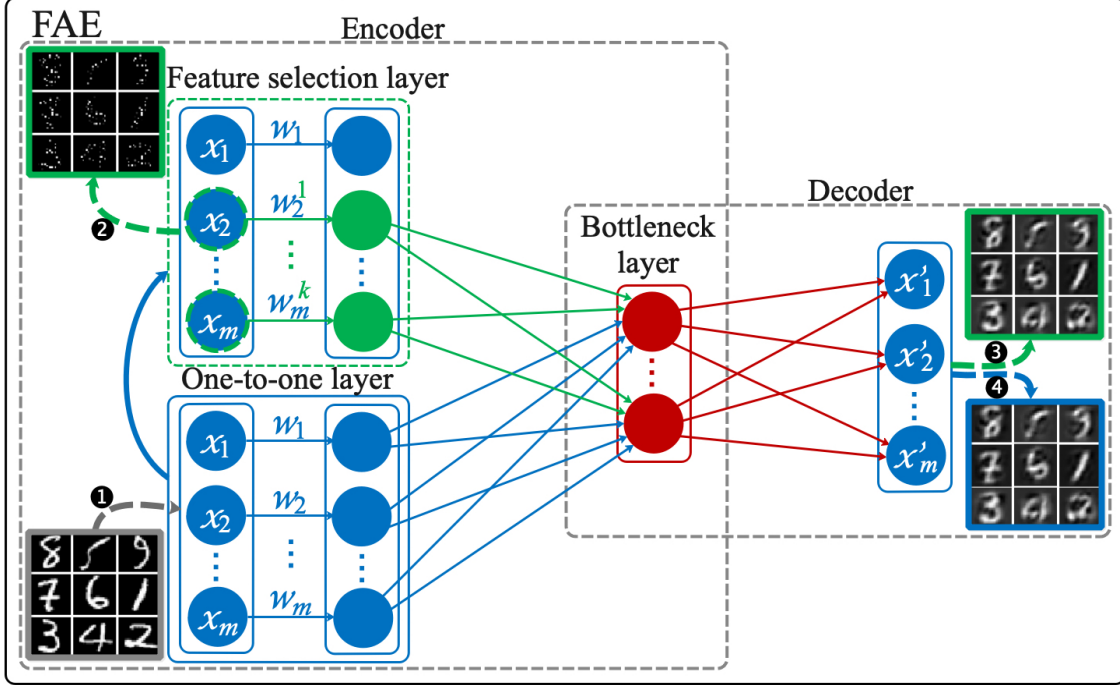


Figure 1: The architecture of FAE. During training, the global NN (with one-to-one layer) and its dependence sub-NN (with feature selection layer) are used to optimize (3); during testing, only the trained sub-NN is used to select features and reconstruct the data. Potentially, FAE implements feature extraction. The showed quantifies are: 1) input; 2) feature selection result; 3) reconstruction based on the selected features, i.e., $f(g(\mathbf{X}\mathbf{W}_I^{\max k}))$; 4) reconstruction from the one-to-one layer, i.e., $f(g(\mathbf{X}\mathbf{W}_I))$.

3.4 Identification Autoencoders (IAE)

To perform feature selection in the original space, our first attempt is to add a simple one-to-one layer between the input and hidden layers of AE to weigh the importance of each input feature. It is also natural to exploit the sparsity property of ℓ_1 regularization for the weights of this layer for feature selection, inspired by Lasso [Tibshirani, 1996]. Then, we have the following formulation:

$$\min_{\mathbf{W}_I, f, g} \|\mathbf{X} - f(g(\mathbf{X}\mathbf{W}_I))\|_F^2 + \lambda_1 \|\mathbf{W}_I\|_1, \text{ s.t. } \mathbf{W}_I \geq 0,$$

where $\mathbf{W}_I = \text{Diag}(\mathbf{w})$, $\mathbf{w} \in \mathbb{R}^m$, and λ_1 is a parameter balancing between the reconstruction error and sparsity regularization. The ℓ_1 norm induces sparsity and shrinks the less important features' weights to 0, and it may make the features more discriminative as well. Here, we require that the entries of \mathbf{W}_I should be nonnegative since they represent the importance of the features and the non-negativity constraint would make their interpretation more meaningful [Xu et al., 2019]. The fully connected concrete layer [Abid et al., 2019] has taken a similar non-negativity constraint, albeit for a full matrix.

For AE with such an additional one-to-one layer and the modified objective function, we call it an identification autoencoder (IAE) only for notational purpose. Actually, IAE is a general case of AgnoS-S [Doquet and Sebag, 2019], where it does not impose any constraint on the dimension of the bottleneck layer of AE. After training, the features corresponding to the k largest entries of \mathbf{W}_I are selected as the most informative features. Compared with standard AE, IAE clearly increases no more than m additional parameters.

We may visualize the selected features by IAE in Figure 2 (c) and (e). It is seen that IAE captures a part of key features from the original samples; however, it cannot capture other key features on the skeleton of the digits, and the selected features fail to recover the original contents, as shown in Figure 2 (g). In general, the selected features by unsupervised feature selection are to be representative of the input data, implying that the selected features should reconstruct the original samples well. Thus, IAE cannot serve the purpose of feature selection in itself. Its failure is mainly due to the lack of diversity of its selected features. The ℓ_1 regularization term in IAE may promote the sparsity of the feature weight vector; however, it cannot ensure a sufficient level of diversity needed by a representative subset of features. Because the features in real data often have significant inter-correlations and even redundancy, without

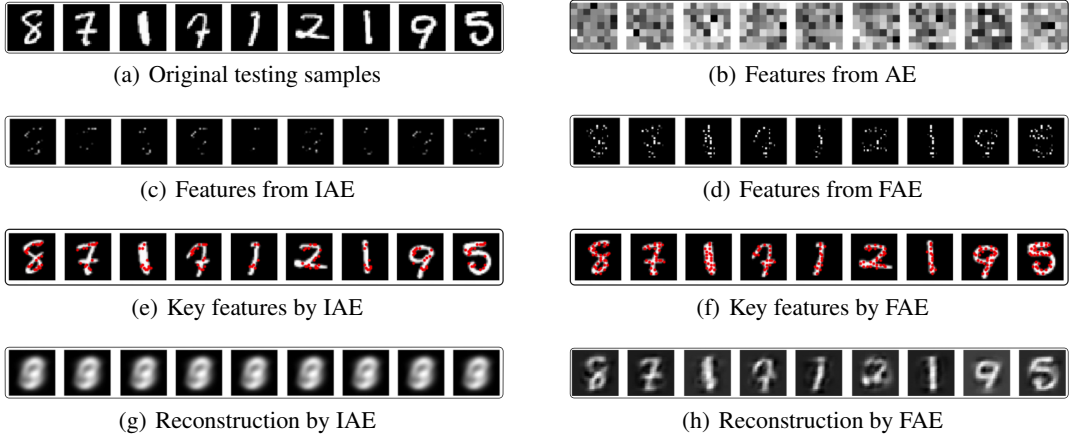


Figure 2: (a) Testing samples randomly chosen from MNIST; (b) 49 features extracted by AE (size enlarged for visualization); (c) 50 features selected by IAE; (d) 50 features selected by FAE; (e) key features by IAE shown with original samples; (f) key features by FAE shown with original samples; (g) IAE’s reconstruction based on the 50 features; (h) FAE’s reconstruction based on the 50 features; (c)-(h) are best viewed with enlarging.

properly taking account of them, the selected features would have high correlations yet lack necessary diversity. Directly computing the pairwise interactions of all features requires a full $m \times m$ weight matrix, which may be computationally costly for high-dimensional data. Accounting for higher-order interactions between features would require even higher complexities. To address this problem, we propose a simple yet effective approach by using a sub-NN to locally excavate for diversity information from the feature weights, thereby reducing the search space significantly. We will introduce this sub-network below, which leads to the architecture of FAE.

3.5 Fractal Autoencoders (FAE)

To remedy the diversity issue of IAE, we further design a sub-NN term, which requires that the subset of k selected features from \mathbf{W}_I should be so diverse as to still represent the global contents of original samples as much as possible. Putting together, our proposed model is as follows:

$$\min_{\mathbf{W}_I, f, g} \|\mathbf{X} - f(g(\mathbf{X}\mathbf{W}_I))\|_{\mathbb{F}}^2 + \lambda_1 \|\mathbf{X} - f(g(\mathbf{X}\mathbf{W}_I^{\max_k}))\|_{\mathbb{F}}^2 + \lambda_2 \|\mathbf{W}_I\|_1, \text{ s.t. } \mathbf{W}_I \geq 0, \quad (3)$$

where $\mathbf{W}_I^{\max_k} = \text{Diag}(\mathbf{w}^{\max_k})$, and λ_1 and λ_2 are nonnegative balancing parameters. We call the neural network corresponding to (3) fractal autoencoders (FAE), due to its seemingly self-similarity characteristic: A small proportion of features in the second term achieve a similar performance to the whole set of features in the first term for reconstructing the original data. This characteristic will be manifested more clearly when applying FAE to extract multiple subsets of features later.

After training FAE, we obtain $\mathbf{W}_I^{\max_k}$ which can be used to perform feature selection on new samples during testing. We illustrate the selected features, the selected features superimposed on the original samples (for easy visualization), and reconstructed samples with these features in (d), (f), and (h) of Figure 2, respectively, for 9 random samples from MNIST.

Because we solve $\mathbf{W}_I^{\max_k}$ by jointly optimizing the global-NN and sub-NN, if we re-optimize the selected features to reconstruct the original data, the reconstruction error is expected to be smaller than that from FAE, which is stated in the following Theorem 1. This theorem shows the potential benefit of re-optimization based on the selected features by FAE. It motivates the later use of the linear regression model on the selected features for GEO. Due to space constraint, the proof of Theorem 1 and its related discussion are provided in the Supplementary Material.

Theorem 1. *Let $(\mathbf{W}_I^*, f^*, g^*)$ be an optimal solution of (3). If $\text{Pos}(\mathbf{W}_I^* - (\mathbf{W}_I^*)^{\max_k}) > 0$, then there exists $(f^{*'}, g^{*'})$, such that*

$$\|\mathbf{X} - f^{*'}(g^{*'}(\mathbf{X}(\mathbf{W}_I^*)^{\max_k}))\|_{\mathbb{F}}^2 \leq \|\mathbf{X} - f^*(g^*(\mathbf{X}(\mathbf{W}_I^*)^{\max_k}))\|_{\mathbb{F}}^2.$$

	Dataset	#Sample	#Feature	#Class
1	Mice Protein	1,080	77	8
2	COIL-20	1,440	400	20
3	Activity	5,744	561	6
4	ISOLET	7,797	617	26
5	MNIST	10,000	784	10
6	MNIST-Fashion	10,000	784	10
7	USPS	9,298	256	10
8	GLIOMA	50	4,434	4
9	leukemia	72	7,070	2
10	pixraw10P	100	10,000	10
11	Prostate_GE	102	5,966	2
12	warpAR10P	130	2,400	10
13	SMK_CAN_187	187	19,993	2
14	arcene	200	10,000	2
15	GEO	111,009	10,463	Null

Table 1: Statistics of datasets.

4 Experiments

In this section, we will perform experiments to extensively assess FAE by comparing it with contemporary methods on many benchmarking datasets.

4.1 Datasets to Be Used

The benchmarking datasets used in this paper are Mice Protein Expression [UCI, 2015], COIL-20 [Nene et al., 1996], Smartphone Dataset for Human Activity Recognition in Ambient Assisted Living [Anguita et al., 2013], ISOLET [UCI, 1994], MNIST [Lecun et al., 1998], MNIST-Fashion [Xiao et al., 2017], GEO², USPS, GLIOMA, leukemia, pixraw10P, Prostate_GE, warpAR10P, SMK_CAN_187, and arcene³. We summarize the statistics of these datasets in Table 1. Following CAE [Abid et al., 2019] and considering the long runtime of UDFS, for MNIST and MNIST-Fashion, we randomly choose 6,000 samples from each training set to train and validate and 4,000 from each testing set for testing. And we randomly split 6,000 samples into training and validation sets at a ratio of 90 : 10. For GEO, we randomly split the preprocessed GEO in the same way as D-GEX [Chen et al., 2016]: 88,807 for training, 11101 for validating, and 11,101 for testing⁴. For other datasets, we randomly split them into training, validation, and testing sets by a ratio of 72 : 8 : 20. More details about the data are provided in the Supplementary Material.

4.2 Design of Experiments

In experiments of FAE, we set the maximum number of epochs to be 1000 for datasets 1-14 and 200 for dataset 15. We initialize the weights of feature selection layer by sampling uniformly from $U[0.999999, 0.9999999]$ and the other layers with the Xavier normal initializer. We adopt the Adam optimizer [Kingma and Ba, 2015] with an initialized learning rate of 0.001. We set λ_1 and λ_2 in (3) to 2 and 0.1, respectively. The details of baseline methods are provided in the Supplementary Material. And in the following experiments, we only use the linear version of FAE for simplicity, that is, $g(\mathbf{X}) = \mathbf{X}\mathbf{W}_E$, $\mathbf{W}_E \in \mathbb{R}^{m \times k}$, and $f(g(\mathbf{X})) = (g(\mathbf{X}))\mathbf{W}_D$, $\mathbf{W}_D \in \mathbb{R}^{k \times m}$. The simple, linear version of FAE can already achieve superior performance, as shown below. The use of more complicated, nonlinear version of FAE may further boost the performance, whose results can be found in the Supplementary Material.

For the number of selected features k , we adopt two options: 1) We take $k = 10$ for Mice Protein dataset, 50 for datasets 2-7 following CAE [Abid et al., 2019], and 64 for high-dimensional datasets 8-14. For all baseline methods, we adopt this option. 2) For FAE, we additionally use fewer features, with $k = 8$ for Mice Protein dataset, 36 for datasets 2-7, and 50 for datasets 8-14, to further show its superior representative ability over competing methods. We set the dimension of the latent space to k and denote FAE with these two options as Opt1 and Opt2, respectively.

Two metrics are used for evaluating the models: 1) reconstruction error, which is measured in mean squared error (MSE); 2) classification accuracy, which is measured by passing the selected features to a downstream classifier as a

²Obtained from https://cbcl.ics.uci.edu/public_data/D-GEX/ [Chen et al., 2016].

³The last eight datasets are from the scikit-feature feature selection repository [Li et al., 2017].

⁴Abid et al. [2019] stated that they used the same preprocessing scheme with D-GEX. Though having the same number of features, we note that their dataset has a slightly different sample size 112, 171 from ours and that in [Chen et al., 2016].

Dataset	LS	SPEC	NDFS	AEFS	UDFS	MCFS	PFA	AgnoS-S	CAE	FAE	
										Opt1	Opt2
Mice Protein	0.603	0.051	0.041	0.783	0.867	0.695	0.871	0.013	0.372	0.012	0.015
COIL-20	0.126	0.413	0.134	0.061	0.116	0.085	0.061	0.038	0.093	0.010	0.013
Activity	0.139	0.127	144.353	0.112	0.173	0.170	0.010	0.010	0.108	0.004	0.005
ISOLET	0.344	0.119	0.129	0.301	0.375	0.471	0.316	0.042	0.299	0.014	0.016
MNIST	0.070	0.068	0.136	0.033	0.035	0.064	0.051	0.051	0.026	0.019	0.025
MNIST-Fashion	0.128	0.107	0.127	0.047	0.133	0.096	0.043	0.024	0.041	0.019	0.023
USPS	3.528	1.120	0.918	0.025	0.034	1.050	0.022	0.017	0.010	0.011	0.021
GLIOMA	0.140	0.210	0.404	0.060	0.060	0.173	0.055	0.054	0.063	0.054	0.189
leukemia	6.978	8.127	7.889	7.751	7.387	20.016	8.568	7.426	4.442	6.370	6.850
pixraw10P	32.758	0.524	0.874	0.002	0.007	0.073	0.003	0.002	0.006	0.004	0.002
ProstateGE	1.694	0.605	4.506	0.280	0.228	1.929	0.180	0.387	0.048	0.208	0.058
warpAR10P	1.187	0.320	0.534	0.034	0.107	2.548	0.035	0.031	0.055	0.028	0.026
SMK_CAN_187	7.344	0.118	3.005	0.102	\	5.492	0.089	0.096	0.077	0.087	0.085
arcene	0.328	0.045	1335.029	0.025	\	4.826	0.042	0.031	0.029	0.023	0.023

Table 2: Linear reconstruction error with selected features by different algorithms. The “\” mark denotes the case with prohibitive running time, where the algorithm ran for more than a week without getting a result and thus was stopped.

Dataset	LS	SPEC	NDFS	AEFS	UDFS	MCFS	PFA	AgnoS-S	CAE	FAE	
										Opt1	Opt2
Mice Protein	0.134	0.245	0.083	0.125	0.139	0.139	0.130	0.519	0.134	0.546	0.440
COIL-20	0.389	0.149	0.212	0.580	0.556	0.635	0.642	0.892	0.586	0.983	0.986
Activity	0.280	0.203	0.188	0.240	0.287	0.295	0.364	0.561	0.420	0.911	0.875
ISOLET	0.407	0.058	0.073	0.576	0.455	0.522	0.622	0.181	0.685	0.898	0.851
MNIST	0.646	0.114	0.138	0.690	0.892	0.807	0.852	0.550	0.906	0.921	0.912
MNIST-Fashion	0.517	0.276	0.138	0.580	0.547	0.513	0.683	0.791	0.677	0.815	0.788
USPS	0.363	0.463	0.119	0.942	0.944	0.126	0.960	0.956	0.955	0.963	0.962
GLIOMA	0.500	0.200	0.400	0.800	0.700	0.400	0.800	0.800	0.500	0.900	0.900
leukemia	0.533	0.467	0.467	0.733	0.800	0.533	0.733	0.667	0.867	0.867	0.733
pixraw10P	0.500	0.100	0.250	1.000	0.950	0.100	1.000	1.000	1.000	1.000	1.000
ProstateGE	0.524	0.476	0.476	0.857	0.905	0.571	0.905	0.762	0.857	0.952	0.905
warpAR10P	0.077	0.077	0.192	0.808	0.577	0.077	0.923	0.462	0.692	0.923	0.846
SMK_CAN_187	0.579	0.658	0.421	0.500	\	0.447	0.658	0.658	0.737	0.763	0.737
arcene	0.625	0.325	0.700	0.750	\	0.625	0.775	0.775	0.775	0.850	0.825
Average	0.434	0.272	0.276	0.656	0.646	0.414	0.718	0.684	0.700	0.878	0.840

Table 3: Classification accuracy with selected features by different algorithms. The mark “\” is used similarly to Table 2.

viable means to benchmark the quality of the selected subset of features. For fair comparison, following CAE [Abid et al., 2019], after selecting the features, we train a linear regression model with no regularization to reconstruct the original features, and the resulting linear reconstruction error is used as the first metric⁵. Meanwhile, for the second metric we use the extremely randomized trees [Geurts et al., 2006] as the classifier.

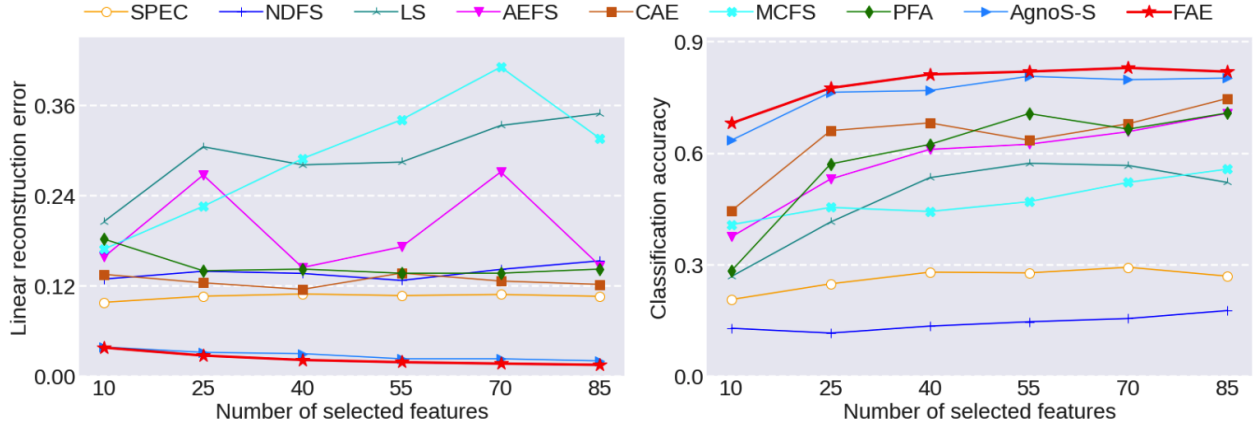
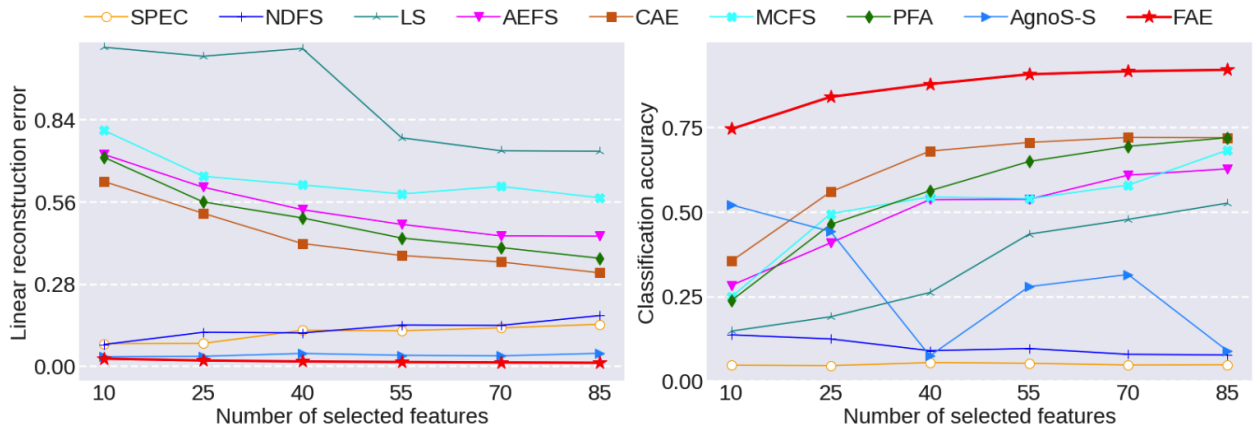
All experiments are implemented with Python 3.7.8, Tensorflow 1.14, and Keras 2.2.5.

4.3 Results on Fourteen Datasets

The experimental results on reconstruction and classification with the selected features by different algorithms are reported in Tables⁶ 2 and 3. For fair comparison, we adopt the available results for reconstruction and classification by LS, AEFS, UDFS, MCFS, PFA, and CAE on datasets 1-6 from [Abid et al., 2019]. From Table 2, it is seen that FAE yields smaller reconstruction errors than baseline methods on majority datasets, indicating its strong ability for representing the original data. From Table 3, it is evident that FAE exhibits consistently superior performance in the downstream classification task on diverse datasets. For visual inspection, the subsets of selected features by FAE for MNIST, MNIST-Fashion, and COIL-20 are depicted in the Supplementary Material. For these image datasets, it can be clearly observed that the selected features comprise the key points on the sample’s skeletons.

⁵For reconstruction error only, it denotes the error from the second term of (3), that is, $\|\mathbf{X} - f(g(\mathbf{X}\mathbf{W}_1^{\max_k}))\|_F^2$.

⁶Except for UDFS on SMK_CAN_187 and arcene whose run-time is prohibitive.

Figure 3: Reconstruction and classification results versus k on MNIST-Fashion.Figure 4: Reconstruction and classification results versus k on ISOLET.

Further, we compare the behaviors of FAE with respect to k with those of the baseline algorithms. By varying k on MNIST-Fashion and ISOLET, we obtain the corresponding linear reconstruction error and classification accuracy rates from FAE. We plot the results in Figures 3 and 4. It is observed that FAE demonstrates persistently better and more stable performance than other algorithms.

4.3.1 Feature Importance

To examine the importance of the features selected by FAE, we rank and partition them into two equal groups. We examine the performance of both groups on the feature selection layer, i.e., $\mathbf{X} \cdot \mathbf{W}_I^{\max_k}$, and directly on the original samples, i.e., $\mathbf{X} \cdot \text{Diag}(\mathbf{1}(\mathbf{w}^{\max_k}))$. The results are shown in Supplementary Figures 18 and 19. We have two observations: 1) The classification accuracy of the first group is generally better than the second group. However, since FAE is unsupervised, some selected features that are essential for reconstruction might not be important for classification. 2) The classification accuracy on the feature selection layer are nearly the same as that on the original samples. Further, we display the results on the feature selection layer and on the original samples for MNIST, MNIST-Fashion, and COIL-20 in the Supplementary Material for visual inspection. The selected features on the original samples generally appear neater than those on the feature selection layer, which is particularly the case for COIL-20, likely because the COIL-20 features have a significant level of redundancy. More discussions can be found in the Supplementary Material.

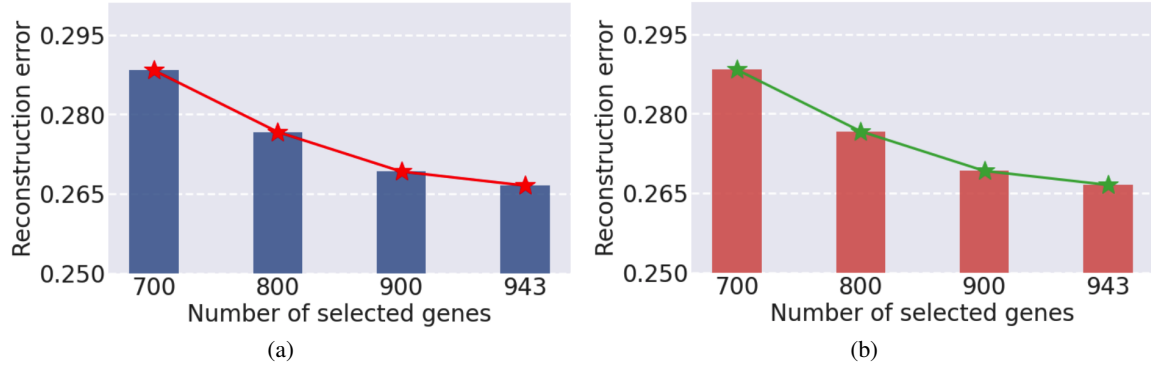


Figure 5: Gene selection by using FAE for GEO. (a) Reconstruction error by FAE; (b) Reconstruction error by using the linear regression model on L1000 landmark genes and FAE-selected genes.

4.4 Analysis of L1000 Gene Expression

It is expensive to measure all gene expressions. To reduce the cost, researchers from the LINCS program⁷ have found that a carefully selected set of genes can capture most gene expression information of the entire human transcriptome because the expression of genes is usually correlated under different conditions. Based on the selected genes, a linear regression model was used to infer the gene expression values of the remaining genes [Chen et al., 2016]. Recently, Abid et al. [2019] have used CAE to further reduce the number of genes to 750 to achieve a similar linear reconstruction error about 0.3 to the original 943 landmark genes of L1000.

Now we apply FAE on the preprocessed GEO to select varying numbers of representative genes from 500 to 943. Figure 5 (a) shows that, by using 600 genes, FAE achieves a reconstruction error better than that with 750 selected genes by CAE. However, CAE uses a slightly different number of samples with ours. For consistency, we mainly compare FAE with L1000. We compute the reconstruction error by using the linear regression model on the genes selected by FAE and the landmark genes of L1000, and the results in MSE are depicted in Figure 5 (b). Evidently, using 800 genes by FAE achieves a similar reconstruction to L1000. Thus, FAE reduces the number of genes by about 15% compared to L1000. The selected genes by FAE and the curves of loss over epochs are displayed in the Supplementary Material. It is observed that, with different numbers of selected genes, a few genes sometimes are selected and sometimes not, which may be attributed to the significant correlations among genes. In addition, when selecting the same number of 943 genes, only 90 genes selected by CAE are among the landmark genes, while 121 by FAE are among the landmark genes. These results indicate that L1000 landmark genes can be significantly enhanced in representation power.

5 An Application of FAE

FAE is applicable and easily extensible to different tasks. Here we show an application of exploiting multiple hierarchical subsets of the key features. Other potential applications are provided in the Supplementary Material.

5.1 h -HFAE

For an image, usually there are many pixels highly correlated with each other. Thus, the subsets of key features might not be unique; indeed, there often exists more than one subset of informative features that can recover the original data well. Excavating these potential subsets of meaningful features is conducive to facilitate data compression [Sousa et al., 2007] and better understand the structure and inter-relationship of the features. Yet, almost all existing feature selection approaches have little ability to explore these potential subsets. To achieve such an ability, we develop an application in the framework of FAE, which selects multiple non-overlapping subsets of representative features. For clarity, we formalize it as follows:

$$\min_{\mathbf{W}_I^{\max_{k,i}}, \mathbf{W}_E, \mathbf{W}_D} \|\mathbf{X} - ((\mathbf{X}\mathbf{W}_I)\mathbf{W}_E)\mathbf{W}_D\|_F^2 + \lambda_0 \|\mathbf{W}_I\|_1 + \sum_{i=1}^h \lambda_i \|\mathbf{X} - ((\mathbf{X}\mathbf{W}_I^{\max_{k,i}})\mathbf{W}_E)\mathbf{W}_D\|_F^2, \text{ s.t. } \mathbf{W}_I \geq 0, \quad (4)$$

⁷See <http://www.lincsproject.org/LINCS/>

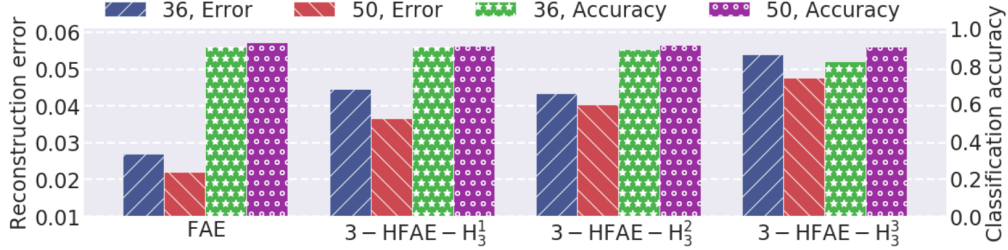


Figure 6: Reconstruction and classification results of FAE and 3-HFAE on MNIST. 3-HFAE-H₃¹, 3-HFAE-H₃², and 3-HFAE-H₃³ denote respectively the first three hierarchical subsets of selected features.

where $\mathbf{W}_I^{\max_k,1} = \text{Diag}(\mathbf{w}^{\max_k,1})$, $\mathbf{W}_I^{\max_k,i} = \text{Diag}((\mathbf{w}/\mathbf{w}^{\max_k,i-1})^{\max_k,i})$, $i = 2, \dots, h$, h is the number of desired subsets of relevant features, $\lambda_i, i = 0, \dots, h$, are hyper-parameters, and $(\mathbf{w}/\mathbf{w}^{\max_k,i-1})^{\max_k,i}$ is an operation to retain the i -th group of k largest entries from \mathbf{w} while making zero all the other entries including the $(i-1)$ groups of k largest entries of $\mathbf{w}^{\max_k,1}, \mathbf{w}^{\max_k,2}, \dots$, and $\mathbf{w}^{\max_k,i-1}$. In (4), the first two terms estimate the importance of each input feature globally; then, the remaining terms organize the top kh features into h hierarchical subsets in descending order of importance values, with each subset having k features. These h subsets are selected by using h sub-NNs, which work together in an orchestrated way: The $(i+1)$ -th sub-NN exploits the $(i+1)$ -th hierarchical subset of features by leaving out the i subsets of features found by the previous i sub-NN(s). For notational convenience, we denote this application for identifying multiple hierarchical subsets of features by h -HFAE. The architecture of h -HFAE is shown in the Supplementary Material.

To verify the effectiveness of h -HFAE, we set $h = 3$ and apply it to MNIST. The reconstruction and classification results together with those of FAE are shown in Figure 6, where we set the hyper-parameters $\lambda_0, \lambda_1, \lambda_2$, and λ_3 in (4) to be 0.05, 1.5, 2, and 3, respectively. With 50 selected features per group, different hierarchies of 3-HFAE achieve almost the same accuracy; with 36 selected features per group, the third group of features from 3-HFAE-H₃³ has slightly worse accuracy than the other two groups. This result implies that 50 selected features per group are more stable for 3-HFAE. For reconstruction error, the vanilla version of FAE is the best among all results.

CAE [Abid et al., 2019] displays the relationships of the top 3 selected features at each node of the concrete selector layer; however, the second and third top features might be insignificant due to the potentially trivial average probability (≤ 0.01). Different from CAE, h -HFAE uses the weights to assign the features into different hierarchical subsets for selection and exploration. In the Supplementary Material, we demonstrate that for 3-HFAE there exists a considerable degree of similarity between different hierarchical subsets of selected features. Thus, h -HFAE can reveal the redundancy or high correlations among features.

6 Conclusions

In this paper, we propose a new framework for unsupervised feature selection, which extends AE by adding a simple one-to-one layer and a sub-NN to achieve both global exploring of representative abilities of the features and local mining for their diversity. Extensive assessment of the new framework has been performed on real datasets. Experimental results demonstrate its superior performance over contemporary methods. Moreover, this new framework is applicable and easily extensible to other tasks and we will further extend it in our future work.

References

- A. Abid, M. F. Balin, and J. Zou. Concrete autoencoders: Differentiable feature selection and reconstruction. In *International Conference on Machine Learning*, pages 444–453, Long Beach, California, United States, June 2019.
- S. Alelyani, J. Tang, and H. Liu. Feature selection for clustering: A review. In C. C. Aggarwal and C. K. Reddy, editors, *Data Clustering: Algorithms and Applications*, chapter 2, pages 29–60. CRC Press, 1st edition, August 2013.
- R. C. Anafi, L. J. Francey, J. B. Hogenesch, and J. Kim. CYCLOPS reveals human transcriptional rhythms in health and disease. *The Proceedings of the National Academy of Sciences*, 114(20):5312–5317, April 2017.
- D. Anguita, A. Ghio, L. Oneto, X. Parra, and J. L. Reyes-Ortiz. A public domain dataset for human activity recognition using smartphones. In *European Symposium on Artificial Neural Networks, Computational Intelligence And Machine Learning*, pages 437–442, Bruges, Belgium, April 2013.
- D. H. Ballard. Modular learning in neural networks. In *National Conference on Artificial Intelligence*, pages 279–284, Seattle, Washington, United States, July 1987.
- R. Bellman. *Dynamic Programming*. Princeton University Press, Princeton, New Jersey, United States, 1st edition, 1957.
- A. Blum, J. Hopcroft, and R. Kannan. *Foundations of Data Science*. Cambridge University Press, Cambridge, United Kingdom, 1st edition, 2020.
- D. Cai, C. Zhang, and X. He. Unsupervised feature selection for multi-cluster data. In *International conference on Knowledge discovery and data mining*, pages 333–342, Washington, District of Columbia, United States, July 2010.
- Y. Chen, Y. Li, R. Narayan, A. Subramanian, and X. Xie. Gene expression inference with deep learning. *Bioinformatics*, 32(12):1832–1839, February 2016.
- R. Clarke, H. W. Ransom, A. Wang, J. Xuan, M. C. Liu, E. A. Gehan, and Y. Wang. The properties of high-dimensional data spaces: implications for exploring gene and protein expression data. *Nature Reviews Cancer*, 8(1):37–49, January 2008.
- G. Doquet and M. Sebag. Agnostic feature selection. In *Joint European Conference on Machine Learning and Knowledge Discovery in Databases*, pages 343–358, Würzburg, Germany, September 2019.
- P. Geurts, D. Ernst, and L. Wehenkel. Extremely randomized trees. *Machine learning*, 63(1):3–42, March 2006.
- I. Guyon and A. Elisseeff. An introduction to variable and feature selection. *Journal of Machine Learning Research*, 3(7-8):1157–1182, March 2003.
- Y. Hamo and S. Markovitch. The COMPSET algorithm for subset selection. In *International Joint Conference on Artificial Intelligence*, pages 728–733, Edinburgh, Scotland, United Kingdom, July-August 2005.
- K. Han, Y. Wang, C. Zhang, C. Li, and C. Xu. Autoencoder inspired unsupervised feature selection. In *International Conference on Acoustics, Speech and Signal Processing*, pages 2941–2945, Calgary, Alberta, Canada, April 2018.
- X. He, D. Cai, and P. Niyogi. Laplacian score for feature selection. In *Advances in Neural Information Processing Systems*, pages 507–514, Vancouver, British Columbia, Canada, December 2005.
- P. Ji, T. Zhang, H. Li, M. Salzmann, and I. Reid. Deep subspace clustering networks. In *Advances in Neural Information Processing Systems*, pages 23–32, Long Beach, California, United States, December 2017.
- D. P. Kingma and J. L. Ba. Adam: A method for stochastic optimization. In *International Conference for Learning Representations*, San Diego, California, USA, May 2015.
- D. P. Kingma and M. Welling. Auto-encoding variational bayes. *arXiv:1312.6114v10*, <https://arxiv.org/abs/1312.6114>, May 2014.
- Y. Lecun, L. Bottou, Y. Bengio, and P. Haffner. Gradient-based learning applied to document recognition. *Proceedings of the IEEE*, 86(11):2278–2324, November 1998.
- J. Li, K. Cheng, S. Wang, F. Morstatter, R. P. Trevino, J. Tang, and H. Liu. Feature selection: A data perspective. *ACM Computing Surveys*, 50(6):94, December 2017.
- Z. Li, Y. Yang, J. Liu, X. Zhou, and H. Lu. Unsupervised feature selection using nonnegative spectral analysis. In *AAAI Conference on Artificial Intelligence*, pages 1026–1032, Toronto, Ontario, Canada, July 2012.
- Y. Lu, I. Cohen, X. S. Zhou, and Q. Tian. Feature selection using principal feature analysis. In *International conference on Multimedia*, pages 301–304, Augsburg, Bavaria, Germany, September 2007.
- C. J. Maddison, A. Mnih, and Y. W. Teh. The concrete distribution: A continuous relaxation of discrete random variables. *arXiv: 1611.00712v3*, <https://arxiv.org/abs/1611.00712>, March 2017.

- B. K. Natarajan. Sparse approximate solutions to linear systems. *SIAM Journal on Computing*, 24(2):227–234, April 1995.
- S. A. Nene, S. K. Nayar, and H. Murase. Columbia object image library (COIL-20). Technical Report CU-CS-005-96, Department of Computer Science, Columbia University, New York, United States, February 1996.
- K. Pearson. LIII. On lines and planes of closest fit to systems of points in space. *The London, Edinburgh, and Dublin Philosophical Magazine and Journal of Science*, 2(11):559–572, November 1901.
- D. E. Rumelhart, G. E. Hinton, and R. J. Williams. Learning internal representations by error propagation. ICS Report 8506, Institute for Cognitive Science, University of California, San Diego, La Jolla, California, United States, September 1985.
- C. M. Sousa, A. B. Cavalcante, D. Guilhon, and A. K. Barros. Image compression by redundancy reduction. In *International conference on Independent component analysis and signal separation*, pages 422–429, London, United Kingdom, September 2007.
- R. Tibshirani. Regression shrinkage and selection via the lasso. *Journal of the Royal Statistical Society. Series B (Methodological)*, 58(1):267–288, 1996.
- UCI. Machine learning repository. ISOLET data set. <http://archive.ics.uci.edu/ml/datasets/ISOLET>, September 1994.
- UCI. Machine learning repository. Mice protein expression data set. <http://archive.ics.uci.edu/ml/datasets/Mice+Protein+Expression>, August 2015.
- H. Xiao, K. Rasul, and R. Vollgraf. Fashion-MNIST: a novel image dataset for benchmarking machine learning algorithms. *arXiv: 1708.07747v2*, <https://arxiv.org/pdf/1708.07747.pdf>, September 2017.
- J. Xie, R. Girshick, and A. Farhadi. Unsupervised deep embedding for clustering analysis. In *International Conference on Machine Learning*, pages 478–487, New York, United States, June 2016.
- J. Xu, M. Yu, L. Shao, W. Zuo, D. Meng, L. Zhang, and D. Zhang. Scaled simplex representation for subspace clustering. *IEEE Transactions on Cybernetics*, pages 1–13, October 2019.
- Y. Yang, H. T. Shen, Z. Ma, Z. Huang, and X. Zhou. $\ell_{2,1}$ -norm regularized discriminative feature selection for unsupervised learning. In *International Joint Conference on Artificial Intelligence*, pages 1589–1594, Barcelona, Catalonia, Spain, July 2011.
- Z. Zhao and H. Liu. Spectral feature selection for supervised and unsupervised learning. In *International Conference on Machine Learning*, pages 1151–1157, Corvallis, Oregon, United States, June 2007.

Supplementary Material of “Fractal Autoencoders for Feature Selection”

1 Datasets used in experiments

The benchmarking datasets used in this paper are as follows:

MNIST [Lecun et al., 1998] has a training set of 60,000 collected handwritten digits as well as a test set of 10,000 examples, each digitized to a 28×28 grayscale image.

MNIST-Fashion [Xiao et al., 2017] is a dataset of Zalando’s article images, and it has the same image size and structure of training and testing splits as MNIST.

COIL-20 [Nene et al., 1996] consists of 1,440 samples. Each sample is a 128×128 grayscale image. In a similar way to that in CAE [Abid et al., 2019], we resize the original size of images to 20×20 .

ISOLET [UCI, 1994] is a dataset of predicting which letter-name was spoken. The features include spectral coefficients, contour features, sonorant features, per sonorant features, and post-sonorant features. The number of samples is 7797 and the number of features is 617.

Smartphone Dataset for Human Activity Recognition (HAR) in Ambient Assisted Living (AAL)⁸ [Anguita et al., 2013] were collected from a smartphone worn around the waist of participants when they performed activities like standing, sitting, laying, walking, walking upstairs, and walking downstairs. It has 5,744 samples and each sample has 561 features.

Mice Protein Expression [UCI, 2015] contains 1,080 samples. These samples consist of 77 expression profiles/features that are measured in the cerebral cortex of normal and Down syndrome mice.

GEO⁹ has 129,158 gene expression profiles from the Affymetrix microarray platform. Each profile corresponds to 22,268 probes/features. We apply the same preprocessing¹⁰ as D-GEX [Chen et al., 2016] to GEO, then it gives a dataset with a sample size of 111,009. Each sample comprises 10,463 genes, which correspond to 9,520 target genes and 943 landmark genes.

The following eight datasets are taken from the scikit-feature feature selection repository <http://featureselection.asu.edu/datasets.php> [Li et al., 2017].

USPS consists of handwritten digits. It has 7,291 training and 2,007 testing images. And the images are 16×16 grayscale pixels.

GLIOMA is a biological dataset. It has 50 instances, each with 4,434 features.

leukemia consists of 72 samples corresponding to gene expression measurements on 72 leukemia patients. Each sample has 7,070 features.

pixraw10P is a face image dataset contains 100 samples and the number of features is 10,000.

Prostate_GE is a dataset from medical applications. It has 102 samples and 5,966 features.

warpAR10P is a face image dataset. It contains 130 samples with 2,400 features.

SMK_CAN_187 is a dataset consisting of gene expression data from smokers with and without lung cancer. It has 187 samples, each with 19,993 features.

arcene is a dataset used to distinguish cancer versus normal patterns from mass-spectrometric data. It has 200 samples, each with 10,000 features.

⁸In this study, we refer to it as Activity.

⁹The original GEO data were accessed on the LINCS Cloud. We obtained GEO from the link https://cbcl.ics.uci.edu/public_data/D-GEX/, which was provided by Chen et al. [2016].

¹⁰We migrated the D-GEX codes for Python 2.7 to 3.6, and fixed the memory leak issue in the original D-GEX codes.

2 Design of experiments related to other methods

The implementations of LS, SPEC, NDFS, UDFS, and MCFS are taken from the scikit-feature feature selection repository <https://github.com/jundongl/scikit-feature.git> [Li et al., 2017]. The implementations of AEFS, PFA, and CAE are taken from [Abid et al., 2019]. For UDFS and AEFS, we search the values of regularization hyper-parameters and report their results with the optimal hyper-parameters according to MSE for reconstruction. For other methods, their hyper-parameters are set to their default values. Additionally, for CAE, we adopt the linear decoder, that is, without hidden layers, for datasets 1-7, use 1-hidden layer decoder for datasets 8-14 and the comparison of different numbers of selected features on MNIST-Fashion and IOSLET. Although we set the maximum number of epochs to 1,000, by weighing the training error and validation error, we use early stopping, e.g., on leukemia for FAE.

The implementation of AgnoS-S follows the settings of [Doquet and Sebag, 2019]: a single hidden layer, tanh activation for both encoder and decoder, and Adam with an initialized learning rate of 10^2 . For the regularization parameter, it is set to 1. Since the intrinsic dimension is not so easy to obtain practically for some datasets, for fair comparison we set the dimension of the bottleneck layer of AE to the number of selected features. The AE weights are also initialized with the Xavier normal initializer as in [Doquet and Sebag, 2019].

All the experiments are implemented with Python 3.7.8, Tensorflow 1.14, or Keras 2.2.5.

3 Subsets of selected features by FAE

The selected features corresponding to two options of 36 and 50 features for MNIST, MNIST-Fashion, and COIL-20 are respectively shown in Figures 7-9.

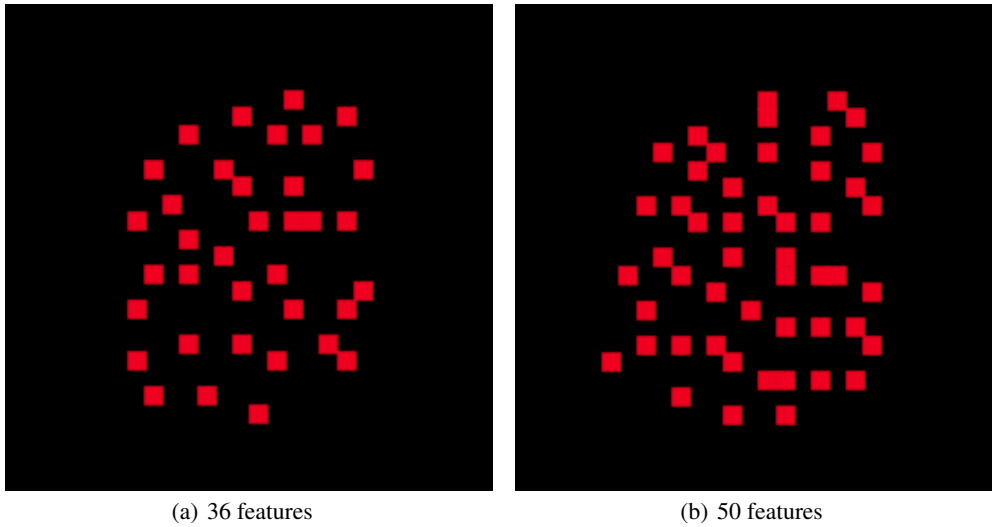


Figure 7: The selected features from 784 pixels on MNIST.

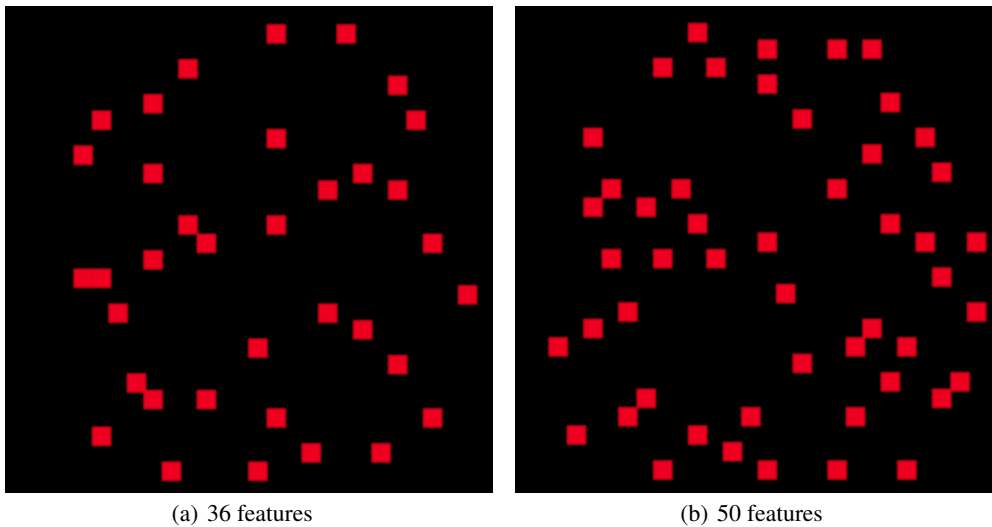
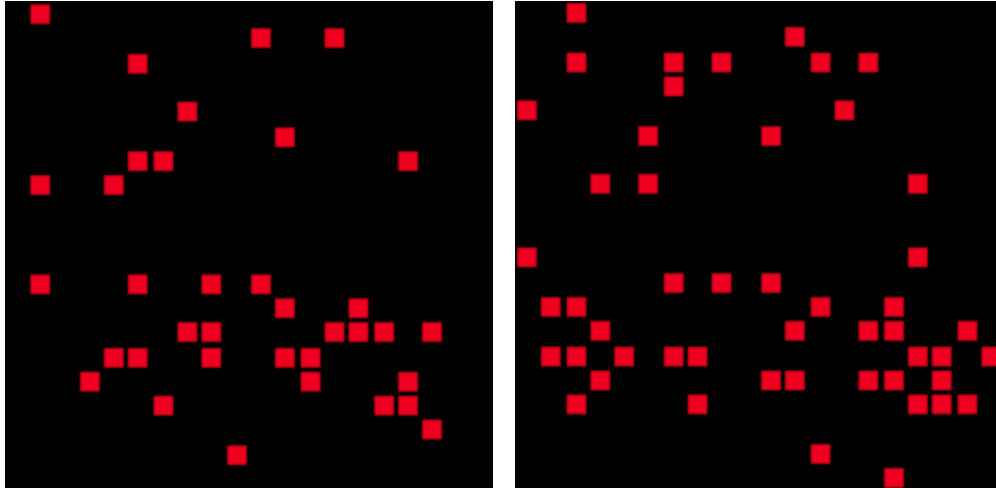


Figure 8: The selected features from 784 pixels on MNIST-Fashion.



(a) 36 features

(b) 50 features

Figure 9: The selected features from 400 pixels on COIL-20.

4 Loss and feature selection for FAE

We present the curves of loss over epochs and feature selection for Opt1 and Opt2. For illustration, we mainly show the results for MNIST, MINST-Fashion, and COIL-20; see Figures 10-15.

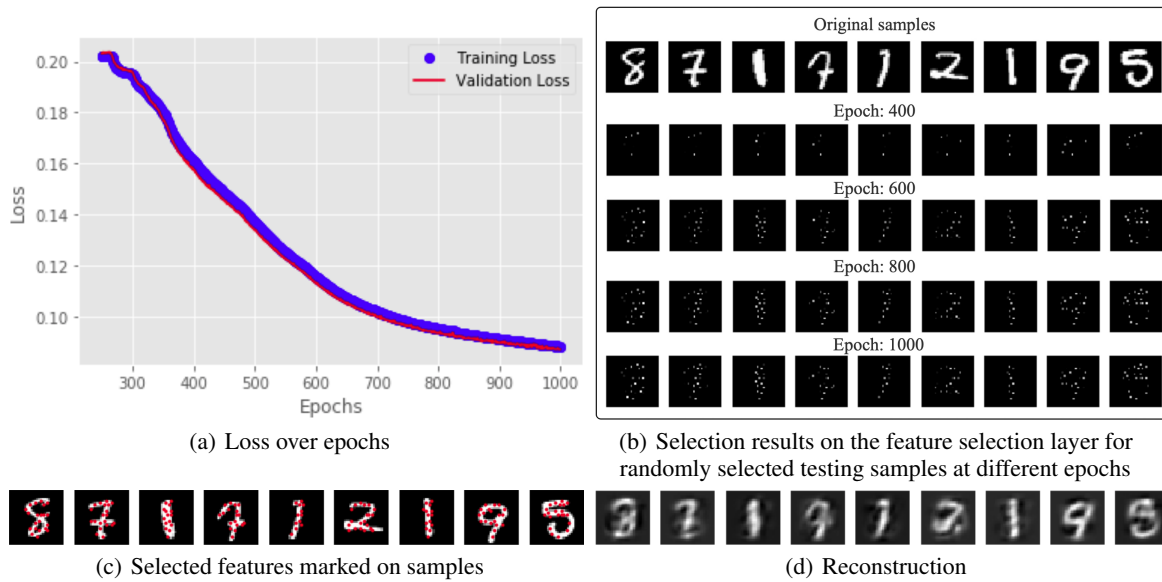


Figure 10: 36 features for MNIST.

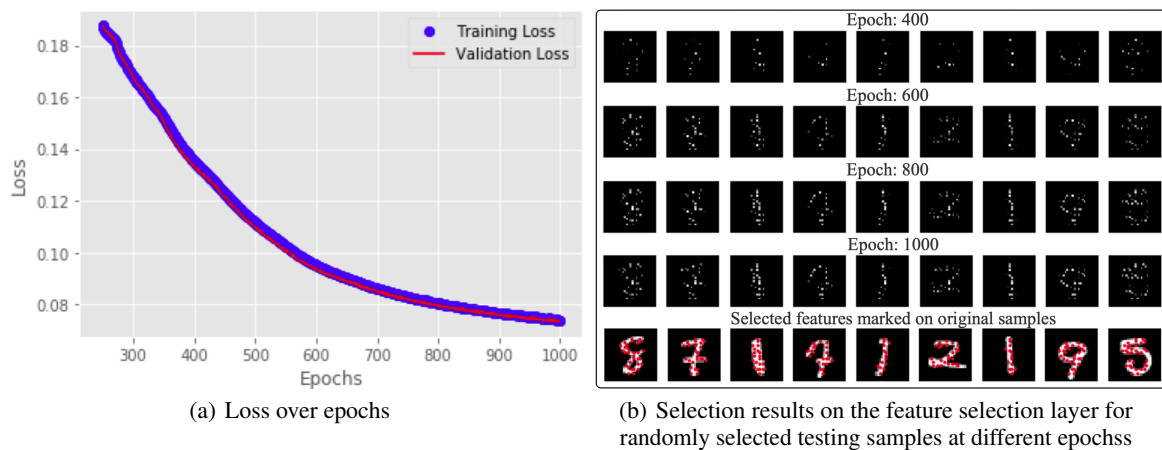


Figure 11: 50 features for MNIST.

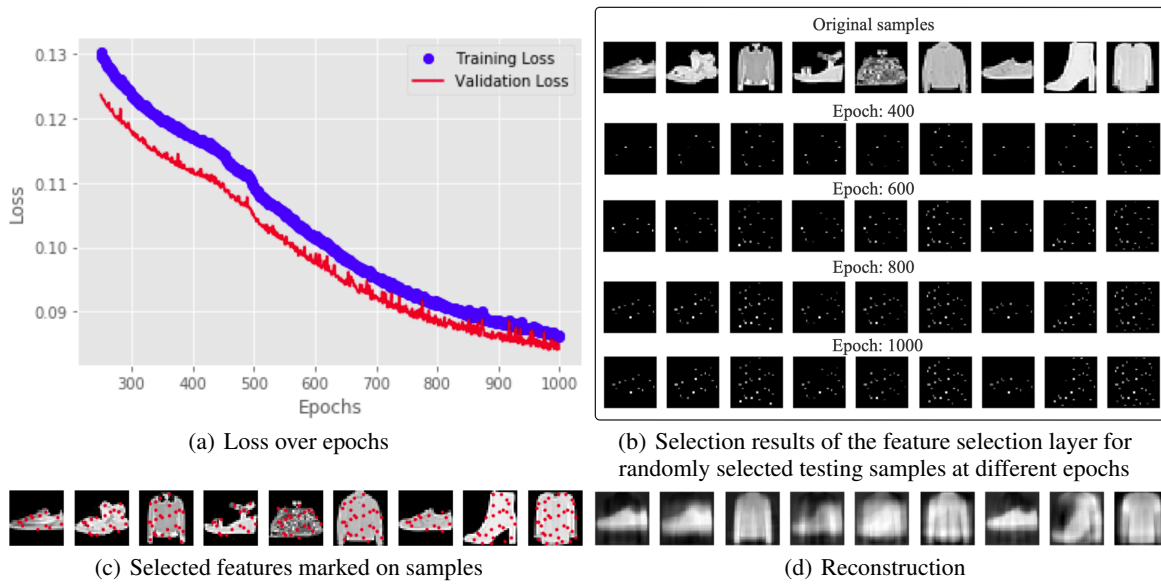


Figure 12: 36 features for MNIST-Fashion.

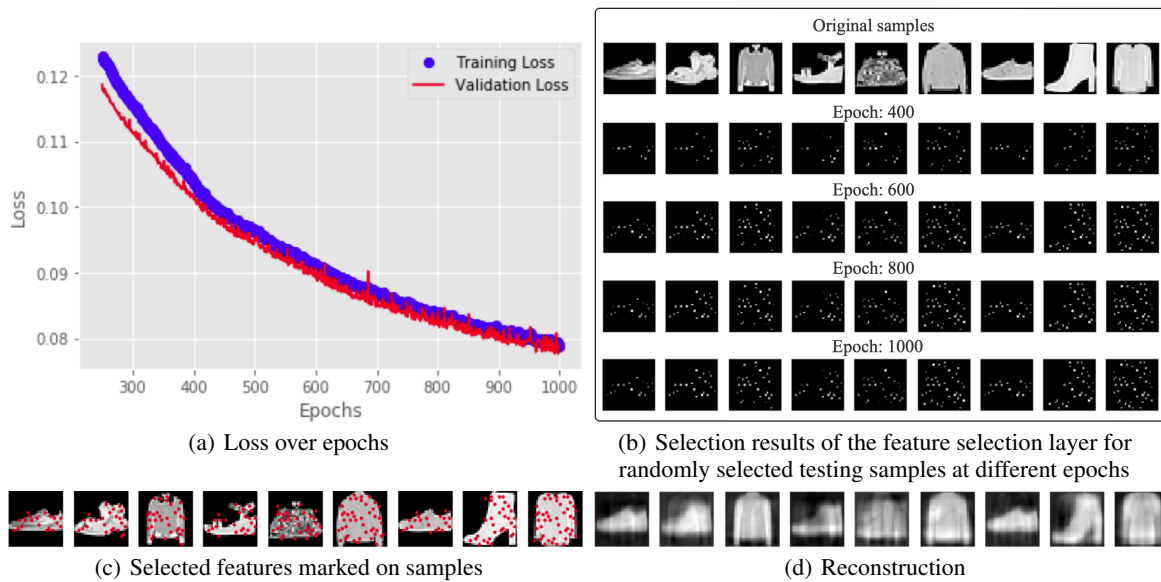


Figure 13: 50 features for MNIST-Fashion.

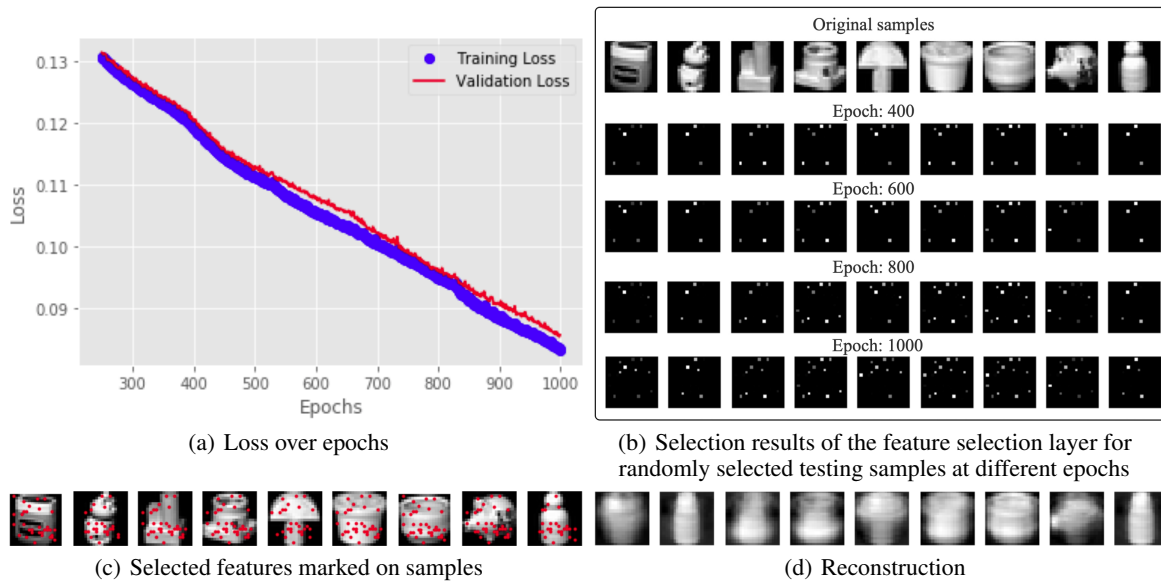


Figure 14: 36 features for COIL-20.

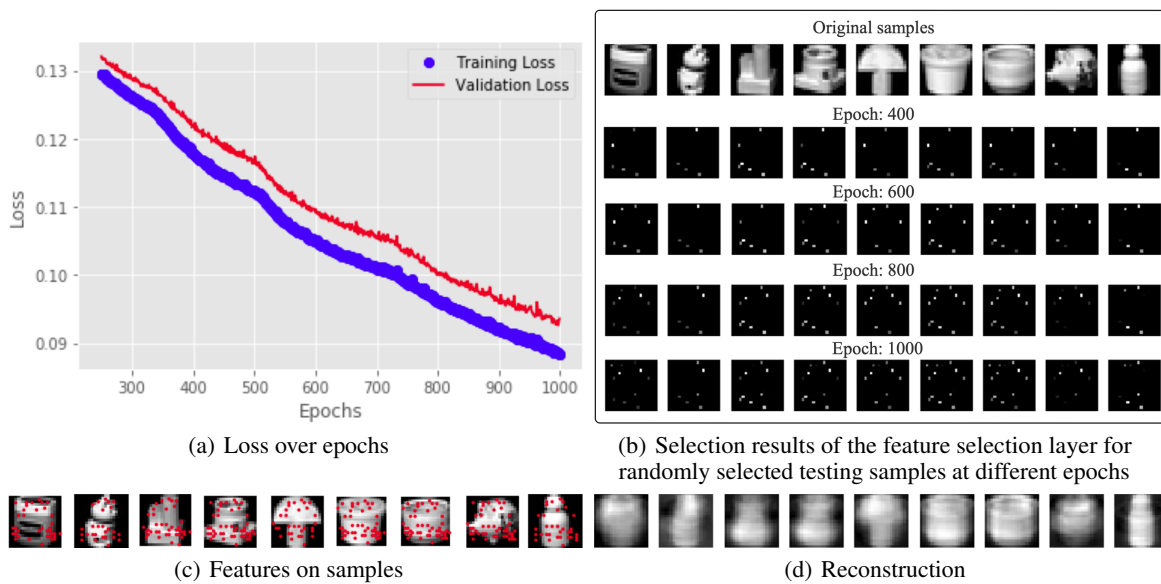


Figure 15: 50 features for COIL-20.

5 Better reconstruction based on selected features

If we use the selected features to reconstruct the original data, the reconstruction error might be smaller than that from FAE, that is, the second term of (3). Such a fact is revealed by the following Theorem. For simplicity, let $A(f, g) = \|\mathbf{X} - f(g(\mathbf{X}\mathbf{W}_I))\|_F^2$, and $B(f, g) = \|\mathbf{X} - f(g(\mathbf{X}\mathbf{W}_I^{\max_k}))\|_F^2$. The proof of Theorem 1 is as follows:

Proof. Assume that, for any $(f^{*''}, g^{*''})$,

$$B(f^{*''}, g^{*''}) > B(f^*, g^*).$$

If (f^*, g^*) is the optimal solution of A , noting that $\text{Pos}(\mathbf{W}_I^* - (\mathbf{W}_I^*)^{\max_k}) > 0$, then there exists $(f^{*'''}, g^{*'''})$, such that

$$B(f^{*'''}, g^{*'''}) \leq B(f, g).$$

This contradicts our assumption. □

We implement experiments to verify Theorem 1 on MNIST, MNIST-Fashion, and COIL-20. The results are shown in Figures 16 and 17 where those based on Theorem 1 are denoted by ‘‘Better’’.

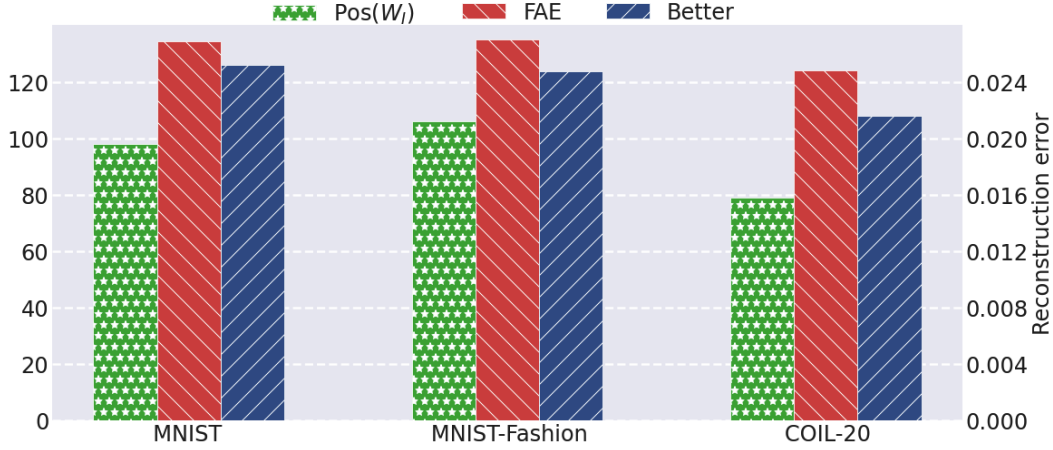


Figure 16: Comparisons of FAE and the better case when $k = 36$.

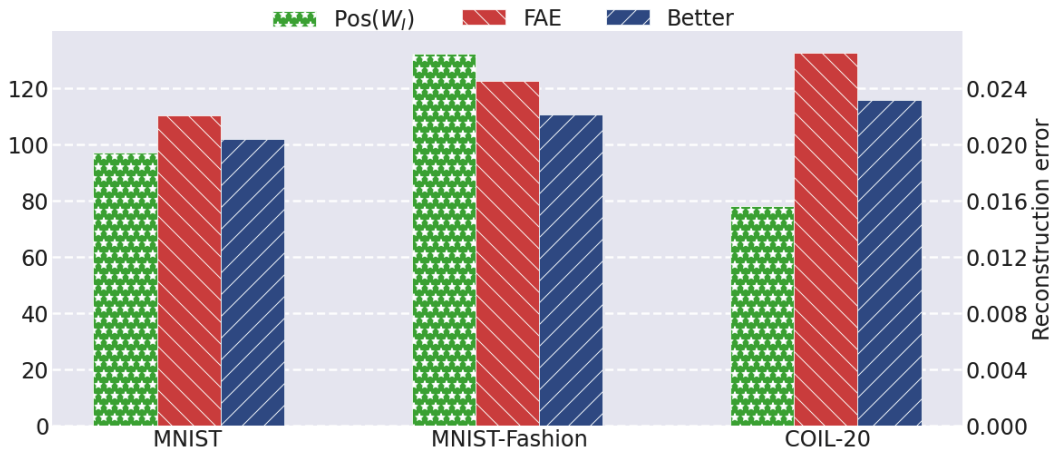


Figure 17: Comparisons of FAE and the better case when $k = 50$.

6 Feature importance

We rank the selected features and partition them into two equal groups. For 36 selected features, each group has 18 features; for 50 selected features, each group has 25 features. On Mice Protein dataset, for 8 selected features, each group has 4 features; for 10 selected features, each group has 5 features. The corresponding results are shown in Figures 18 (a) and 19 (a), respectively. Then, we consider the selection happening on two different layers: 1) the selected features on the input layers or original samples, where the selected features are directly obtained according to whether the element in \mathbf{w}^{\max_k} is larger than 0, that is, $\mathbf{X} \cdot \text{Diag}(\mathbf{1}(\mathbf{w}^{\max_k}))$; 2) the selection from the feature selection layer, where the selection is obtained by multiplying the features on original samples with their corresponding weights \mathbf{w}^{\max_k} , i.e., $\mathbf{X} \cdot \mathbf{W}_1^{\max_k}$. The results of these two kinds of selection for $k = 36$ and $k = 50$ are displayed in Figures 18 (b) and 19 (b), respectively.

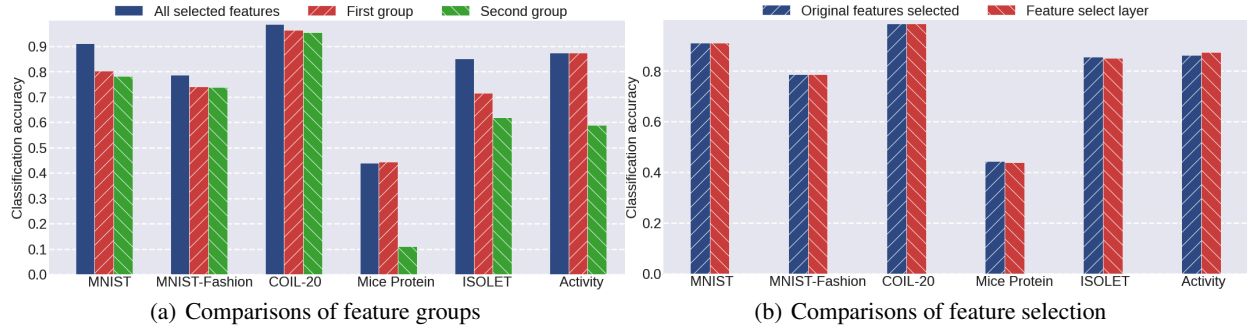


Figure 18: Analyses of feature importance with $k = 36$.

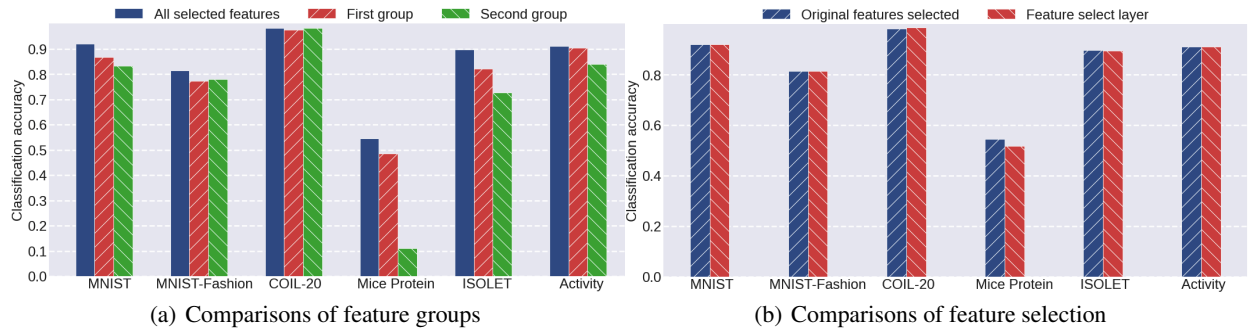


Figure 19: Analyses of feature importance with $k = 50$.

7 Visualization of selected features

We display the selection results on the feature selection layer and the selected features on original samples for MNIST, MNIST-Fashion, and COIL-20 in Figures 20-25, respectively. In Figures 20-23, the selected features on the original samples, i.e., $X \cdot \text{Diag}(\mathbf{1}(\mathbf{w}^{\text{max}_k}))$, are similar to those from the feature selection layer, that is, $X \cdot \mathbf{W}_1^{\text{max}_k}$. However, in Figures 24 and 25, the selected features on the input features are seemingly clearer than those from the feature selection layer. The reason may be that FAE potentially needs fewer selected features to reconstruct the original data for COIL-20, and selecting features directly on the input features may be redundant or highly correlated. But for MNIST and MNIST-Fashion, most of the selected features on the input features are not as correlated as in COIL-20.

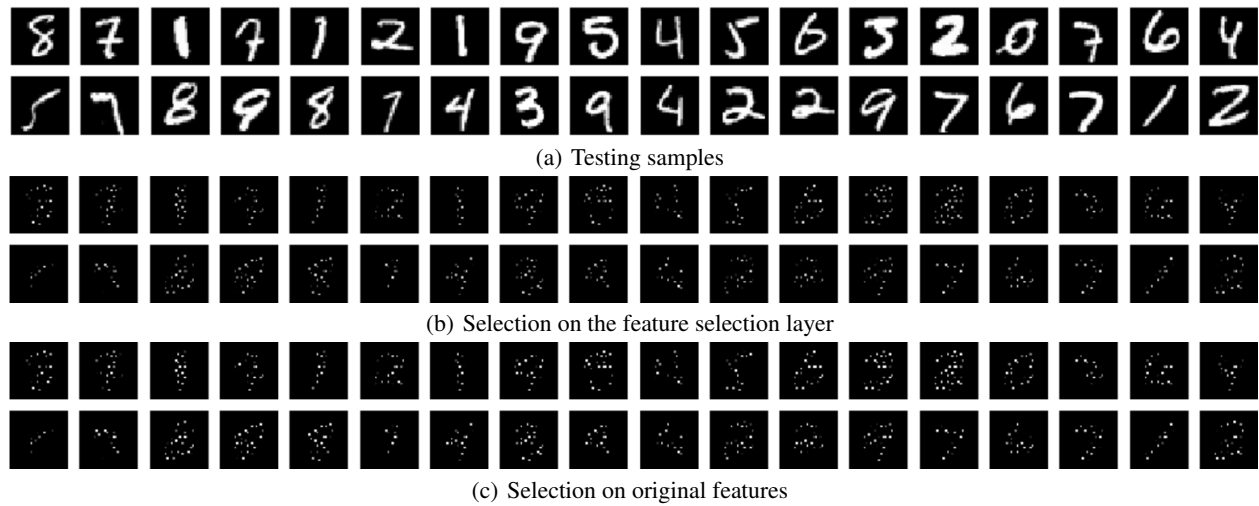


Figure 20: 36 features for MNIST.

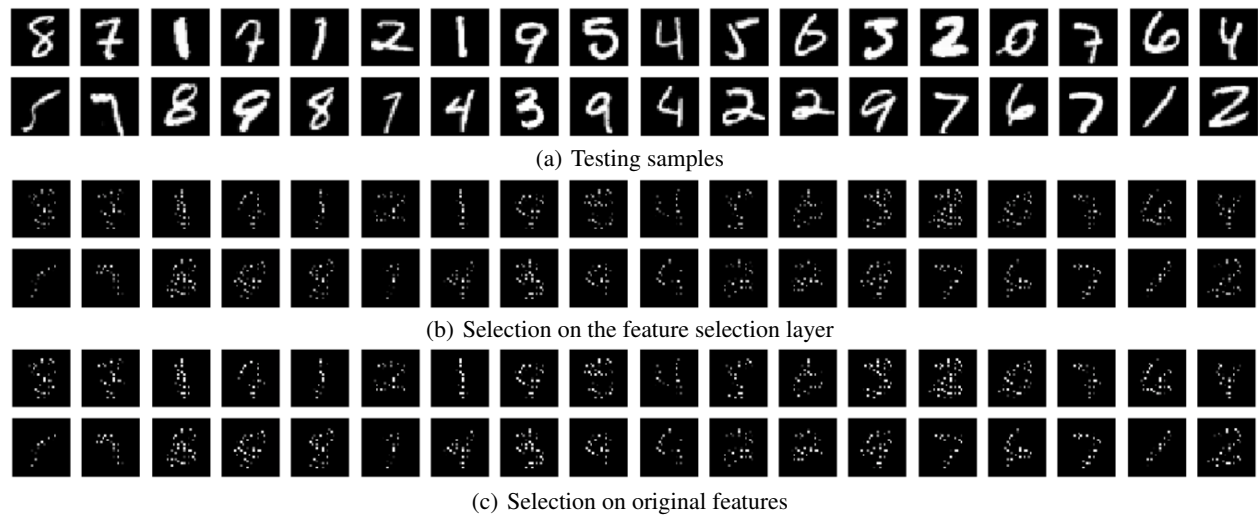


Figure 21: 50 features for MNIST.

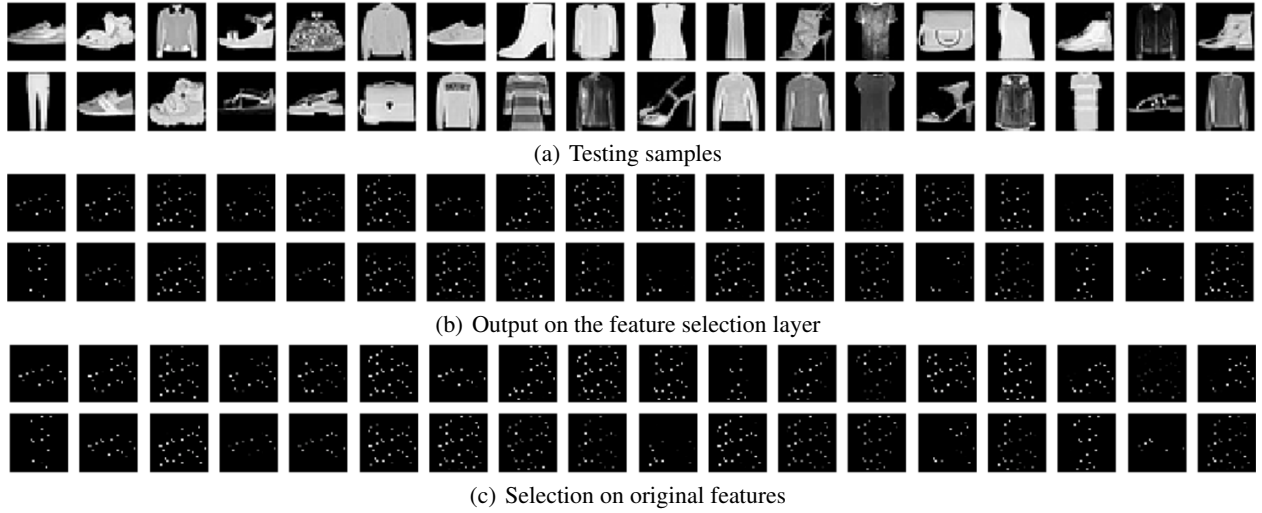


Figure 22: 36 features for MNIST-Fashion.

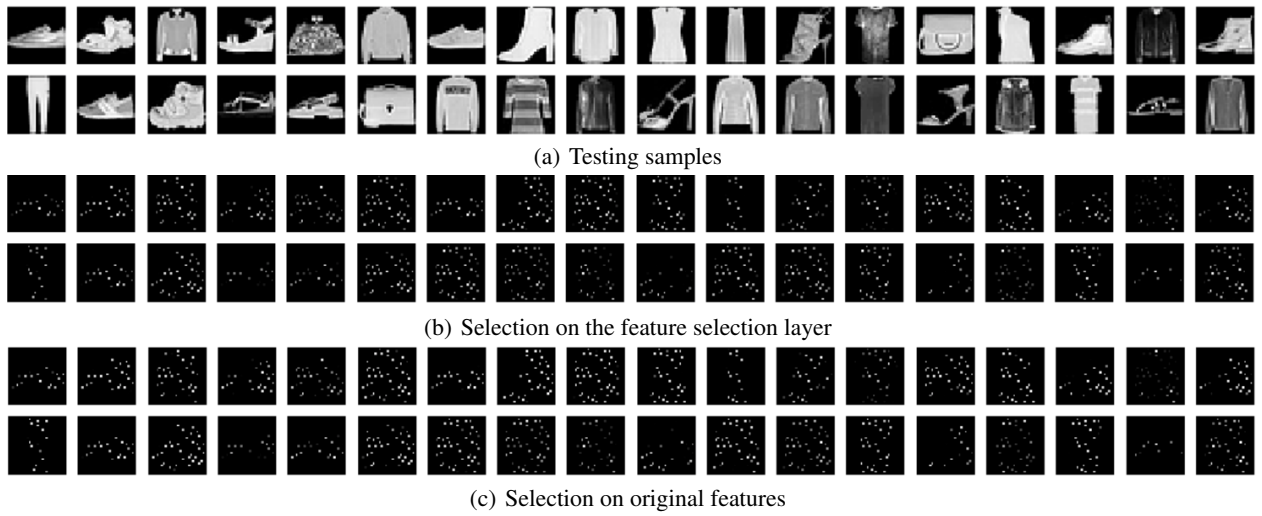


Figure 23: 50 features for MNIST-Fashion.

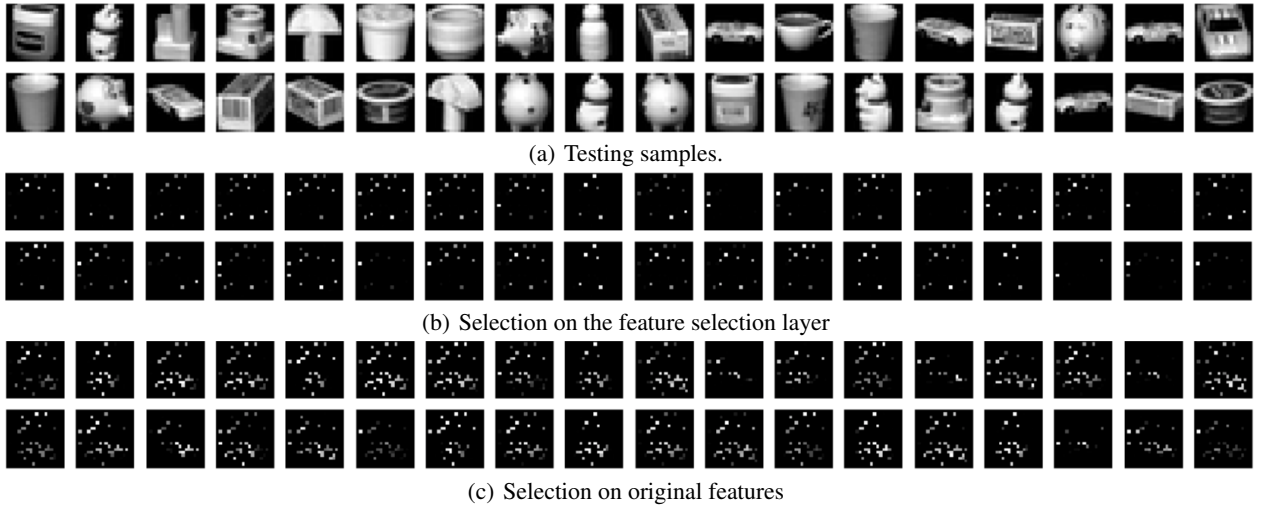


Figure 24: 36 features for COIL-20.

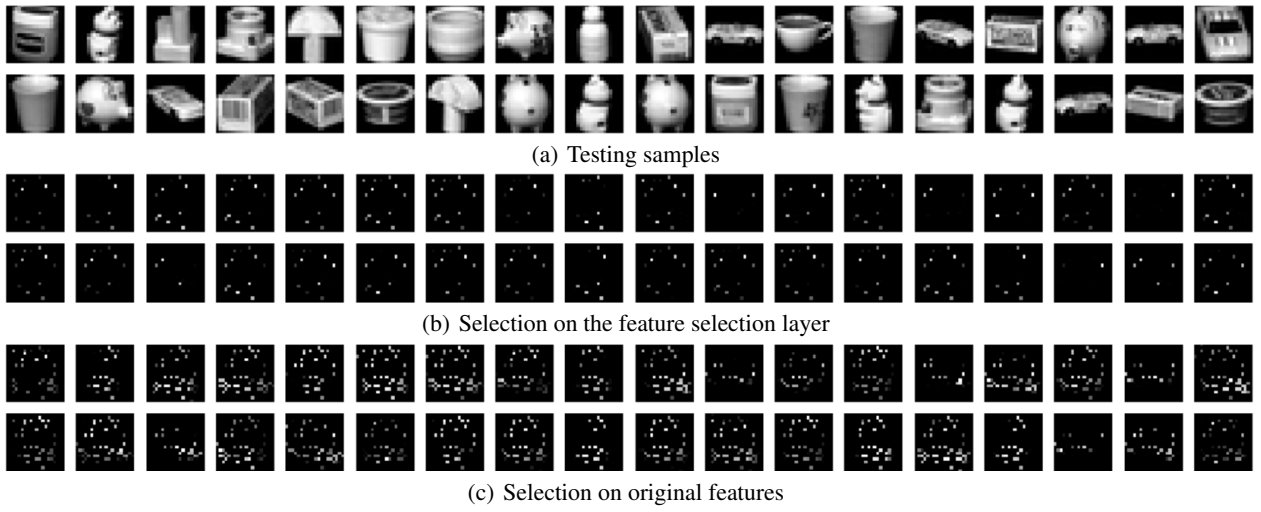
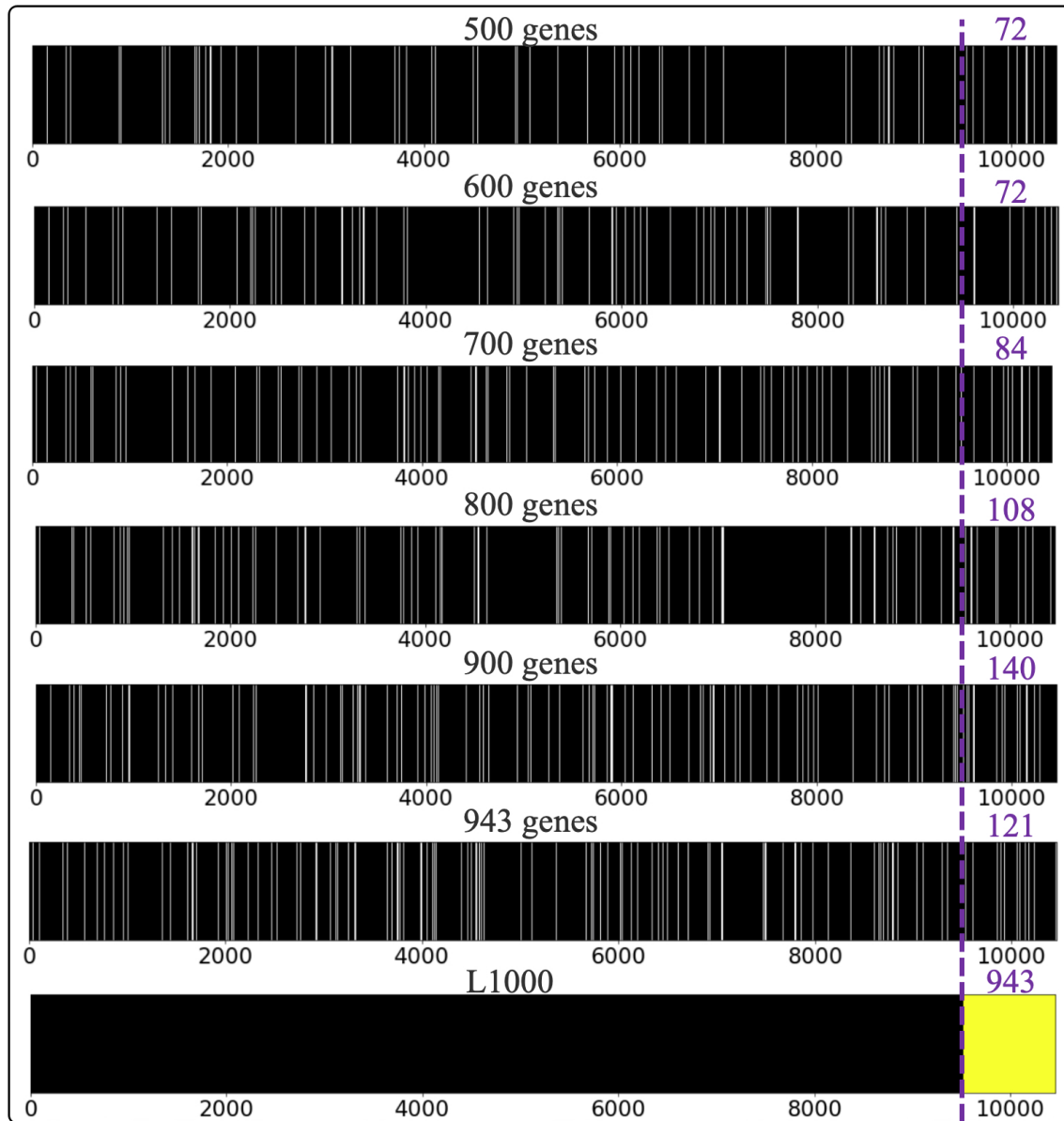


Figure 25: 50 features for COIL-20.

8 Different numbers of selected genes for GEO

We apply FAE to the preprocessed GEO with varying numbers of selected genes, and the results are shown in Figure 26.



(a) Comparison of different numbers of selected genes with 943 landmark genes

Figure 26: Gene selection for GEO. The white lines denote those selected genes by FAE. The purple dashed line separates 943 landmark genes (color coded in yellow) from the other genes. The purple numbers 72, 72, 84, 108, 140, and 121 denote respectively the numbers of overlapping genes between the landmark genes and those selected by FAE with k being 500, 600, 700, 800, 900, and 943.

9 Loss over epochs for GEO

The curves of loss over epochs with different numbers of selected genes are shown in Figure 27.

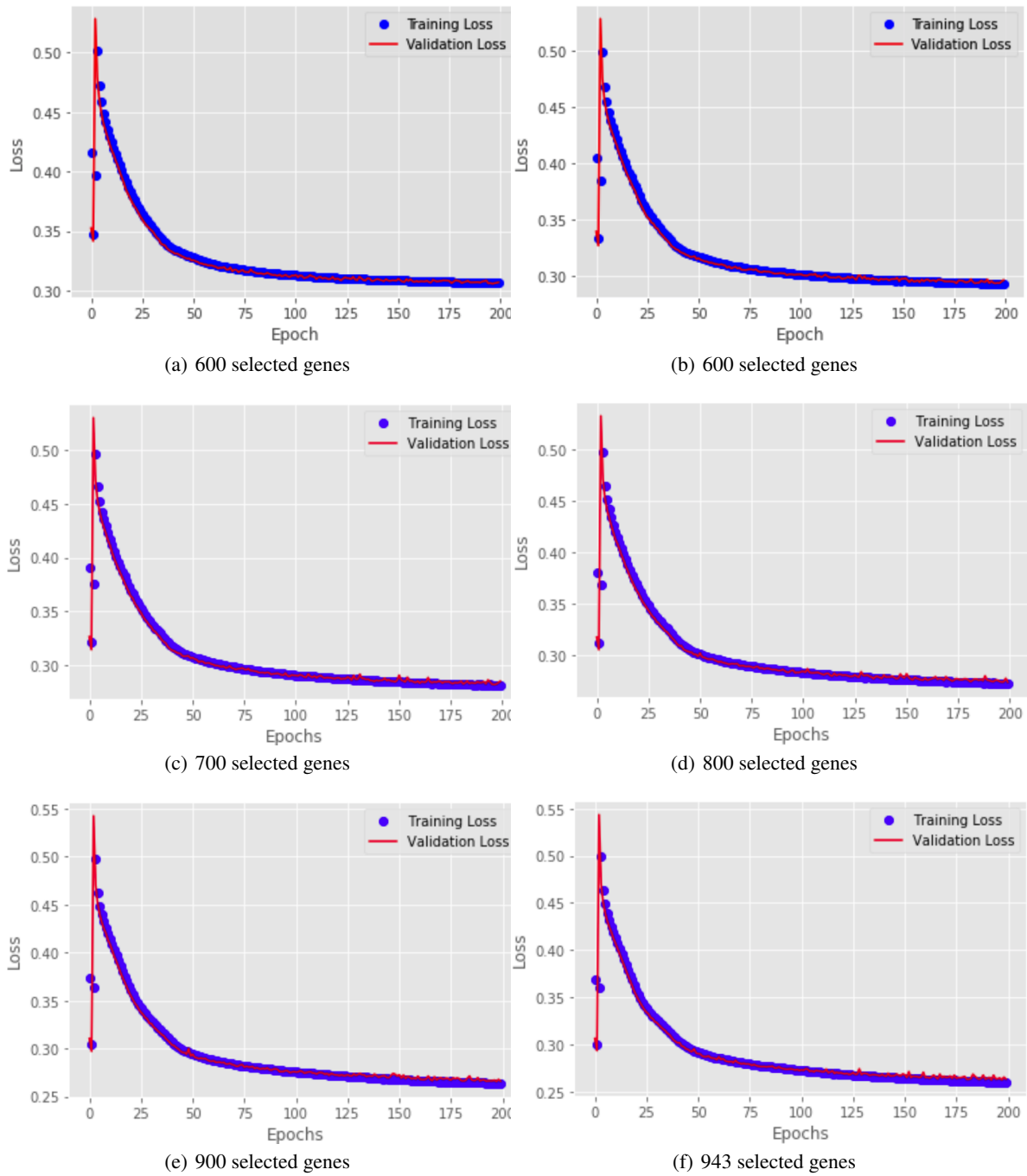


Figure 27: Loss over epoch with different numbers of genes for GEO.

10 Architecture of h -HFAE

The architecture of h -HFAE is shown in Figure 28.

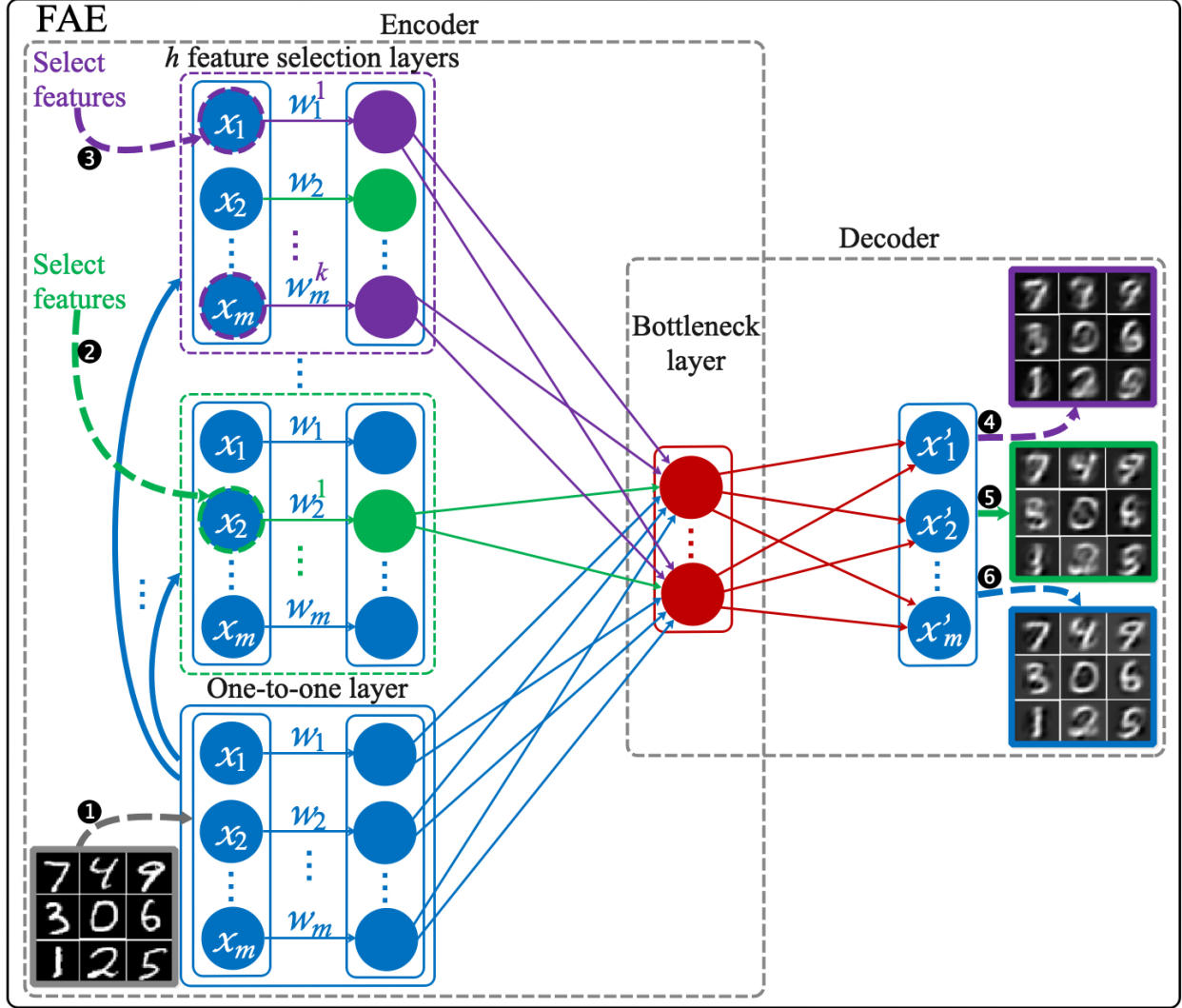


Figure 28: The architecture of h -HFAE. During training, the global NN (with one-to-one layer) and its dependence h sub-NNs (with feature selection layer) are used to optimize Eq. (3); during testing, only the trained h sub-NNs are used to select features and reconstruct the data. The showed quantities of h -HFAE are: 1) input; 2) feature selection for the first-hierarchy subset; 3) feature selection for the h -th-hierarchy subset; 4) reconstruction based on the h -th-hierarchy subset of selected features, i.e., $((\mathbf{X}\mathbf{W}_I^{\max_{k,h}})\mathbf{W}_E)\mathbf{W}_D$; 5) reconstruction based on the first-hierarchy subset of selected features, i.e., $((\mathbf{X}\mathbf{W}_I^{\max_{k,1}})\mathbf{W}_E)\mathbf{W}_D$; 6) reconstruction based on the one-to-one layer, i.e., $((\mathbf{X}\mathbf{W}_I)\mathbf{W}_E)\mathbf{W}_D$.

11 More experimental results of h -HFAE

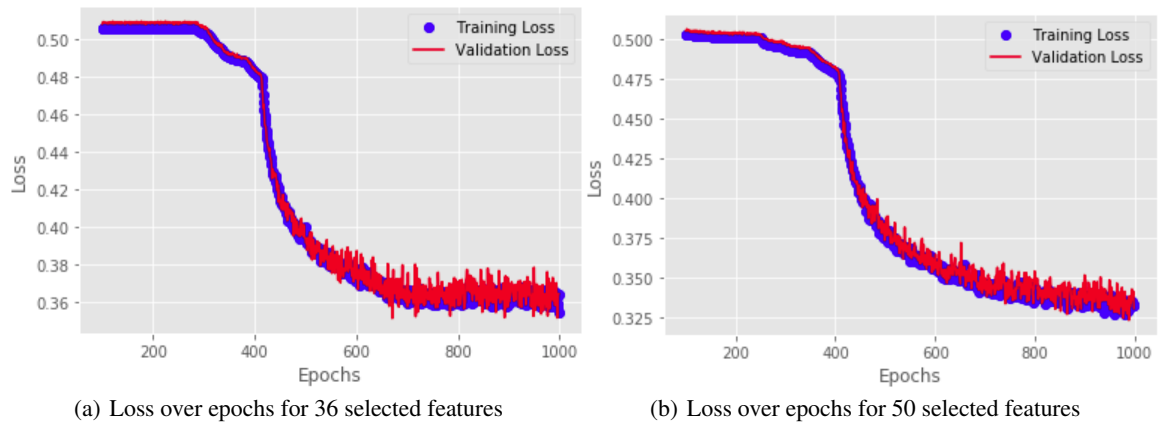


Figure 29: Loss over epochs of 3-HFAE.

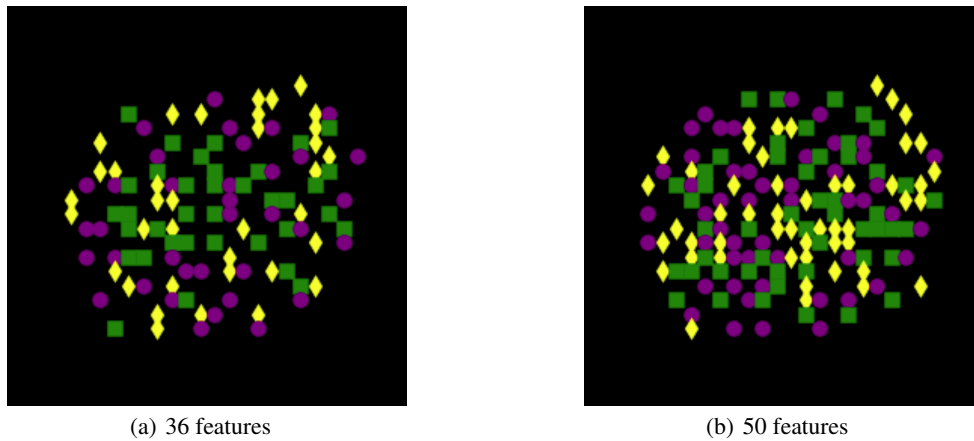


Figure 30: The selected features from 784 pixels on MNIST. The green squares, the purple rounds, and the yellow diamonds respectively denote the first-hierarchy, second-hierarchy, and third-hierarchy subsets of selected features.

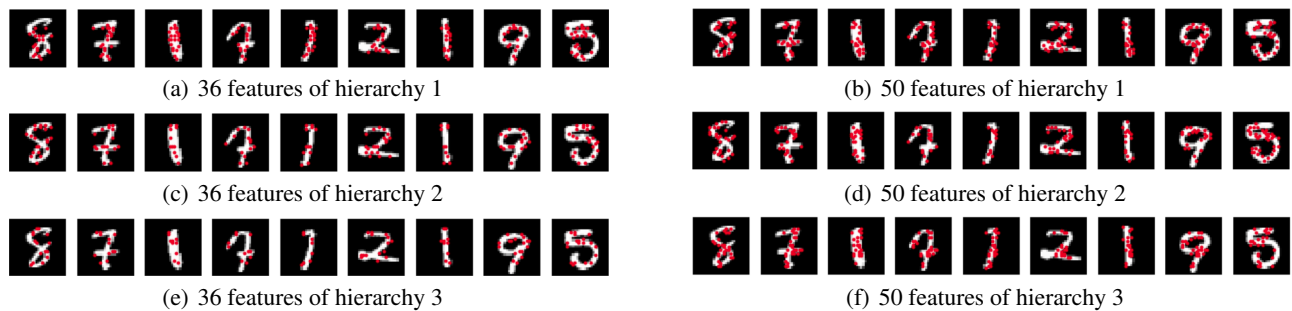


Figure 31: $k = 36$ and $k = 50$ for 3-HFAE. (a)-(f) are all for randomly selected testing samples.

12 Deep nonlinear FAE (DFAE)

To show the performance in the deep and nonlinear case, we apply the following structure in the FAE framework:

$$\min_{\mathcal{F}, \mathbf{W}_I} \|\mathbf{X} - \mathcal{F}(\mathbf{X}\mathbf{W}_I)\|_{\mathbb{F}}^2 + \lambda_1 \|\mathbf{X} - \mathcal{F}(\mathbf{X}\mathbf{W}_I^{\max_k})\|_{\mathbb{F}}^2 + \lambda_2 \|\mathbf{W}_I\|_1 \text{ s.t. } \mathbf{W}_I \geq 0,$$

where $\mathcal{F} = f_3(f_2(f_1(g_3(g_2(g_1(\cdot))))))$. $g_i(\cdot) = \text{ReLU}(\cdot)\mathbf{W}_E^i, i = 1, 2, 3$; $f_i(\cdot) = \text{ReLU}(\cdot)\mathbf{W}_D^i, i = 1, 2$; and $f_3(\cdot) = \text{Sigmoid}(\cdot)\mathbf{W}_E^3$. $\mathbf{W}_E^1 \in \mathbb{R}^{784 \times 128}$, $\mathbf{W}_E^2 \in \mathbb{R}^{128 \times 64}$, $\mathbf{W}_E^3 \in \mathbb{R}^{64 \times k}$, $\mathbf{W}_D^1 \in \mathbb{R}^{k \times 64}$, $\mathbf{W}_D^2 \in \mathbb{R}^{64 \times 128}$, and $\mathbf{W}_D^3 \in \mathbb{R}^{128 \times 784}$. λ_1 and λ_2 are hyper-parameters.

13 Convolutional FAE (CFAE)

To illustrate the application of FAE to images, we apply convolutions in the framework of FAE. Now let \mathbf{Z} be a 2D image and $\mathbf{Z} \in \mathbb{R}^{m \times m}$, for example, if \mathbf{Z} is a sample from MNIST-Fashion, then $m = 28$. For the convolutional case, we have the following extended model:

$$\min_{\mathcal{G}, \overline{\mathbf{W}}} \|\mathbf{Z} - \mathcal{G}(\mathbf{Z} \circ \overline{\mathbf{W}})\|_{\mathbb{F}}^2 + \lambda_1 \|\mathbf{Z} - \mathcal{G}(\mathbf{Z} \circ \overline{\mathbf{W}}^{\max_k})\|_{\mathbb{F}}^2 + \lambda_2 \|\overline{\mathbf{W}}\|_1 \text{ s.t. } \overline{\mathbf{W}} \geq 0,$$

where \circ denotes the Hadamard product, \mathcal{G} is a convolutional network and the structure of \mathcal{G} is given in Figure 32, λ_1 and λ_2 are hyper-parameters, and

$$\overline{\mathbf{W}} = \begin{bmatrix} w_{11} & w_{12} & \cdots & w_{1m} \\ \vdots & \vdots & \ddots & \vdots \\ w_{m1} & w_{m2} & \cdots & w_{mm} \end{bmatrix}, \quad \overline{\mathbf{W}}^{\max_k} = \begin{bmatrix} w_{11}^1 & 0 & \cdots & w_{1m}^i \\ \vdots & \vdots & \ddots & \vdots \\ 0 & 0 & \cdots & w_{mm}^k \end{bmatrix}.$$

Here, $\overline{\mathbf{W}}^{\max_k}$ is an operation to keep the k largest entries in matrix $\overline{\mathbf{W}}$ while making other entries 0.

We apply DFAE and CFAE to MNIST and MNIST-Fashion, respectively. The experimental results are shown in Figures 33, 34, and 35 in Sections 15 and 16, respectively. It can be seen that DFAE and CFAE achieve a better performance than FAE. Here we mainly intend to show the feasibility of extending FAE to deep and convolutional cases. Undoubtedly, one can expect that DFAE and CFAE have advantages due to the strong representation power of deep and convolutional models. Nonetheless, it is worthwhile to note that, with linear FAE, we can already obtain state-of-the-art performance.

14 Architecture of CFAE

The architecture of CFAE is shown in Figure 32. For the last layer, we use the Sigmoid activation function; for the other convolutional layers, we use the ReLU activation function.

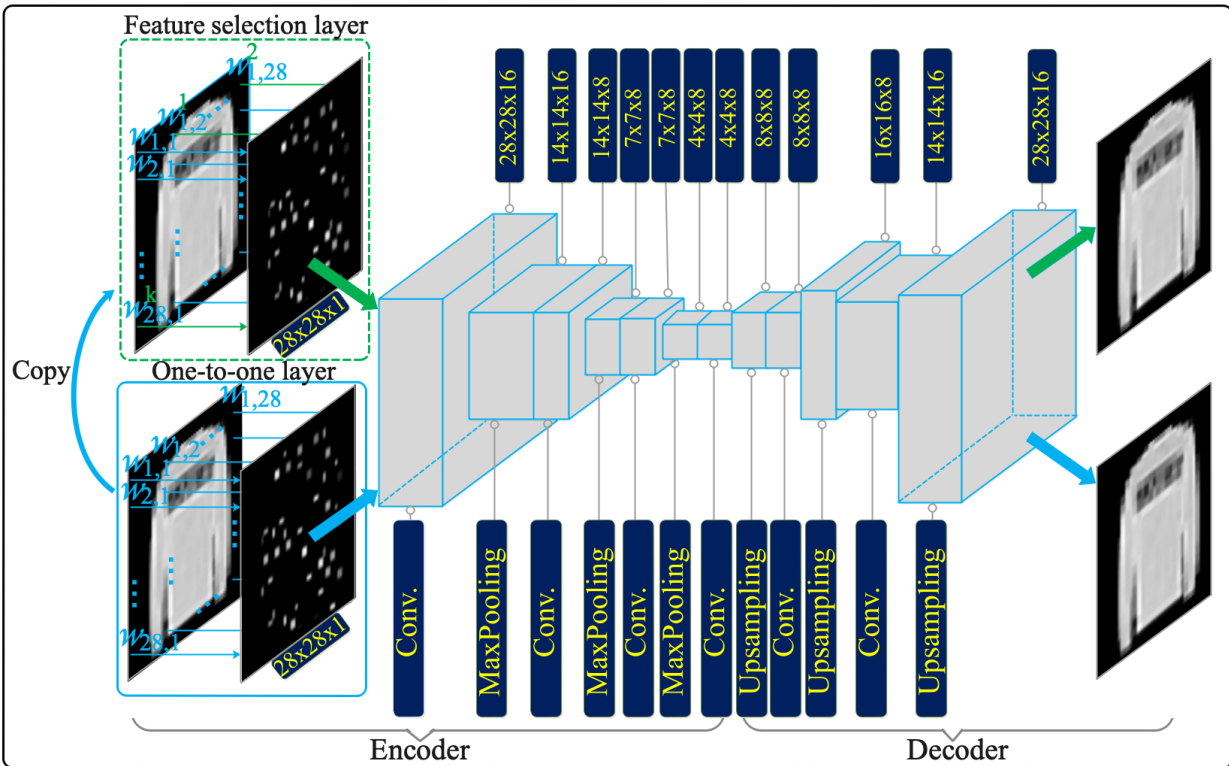


Figure 32: The architecture of CFAE.

15 Reconstruction error and classification accuracy for DFAE and CFAE

The reconstruction error and classification accuracy of DFAE and CFAE over different numbers of selected features are shown in Figure 33.

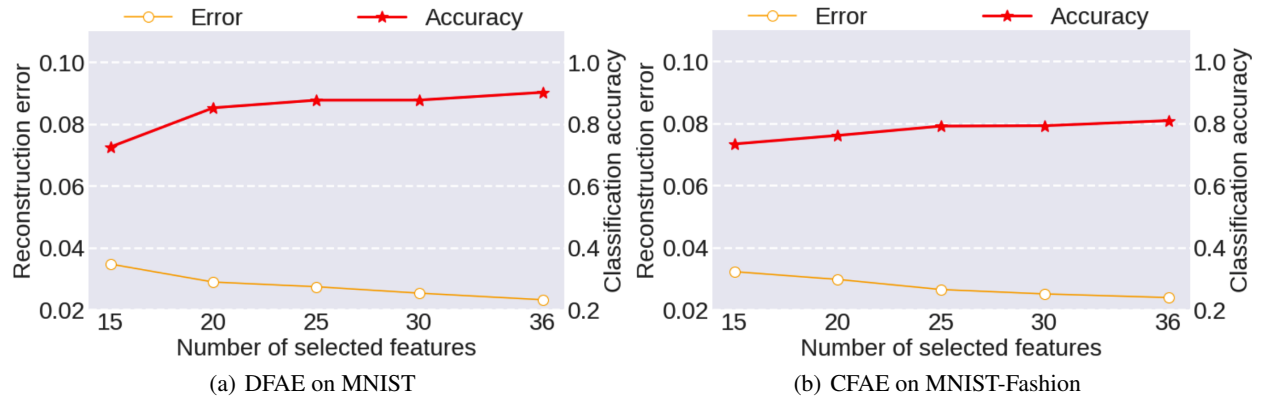
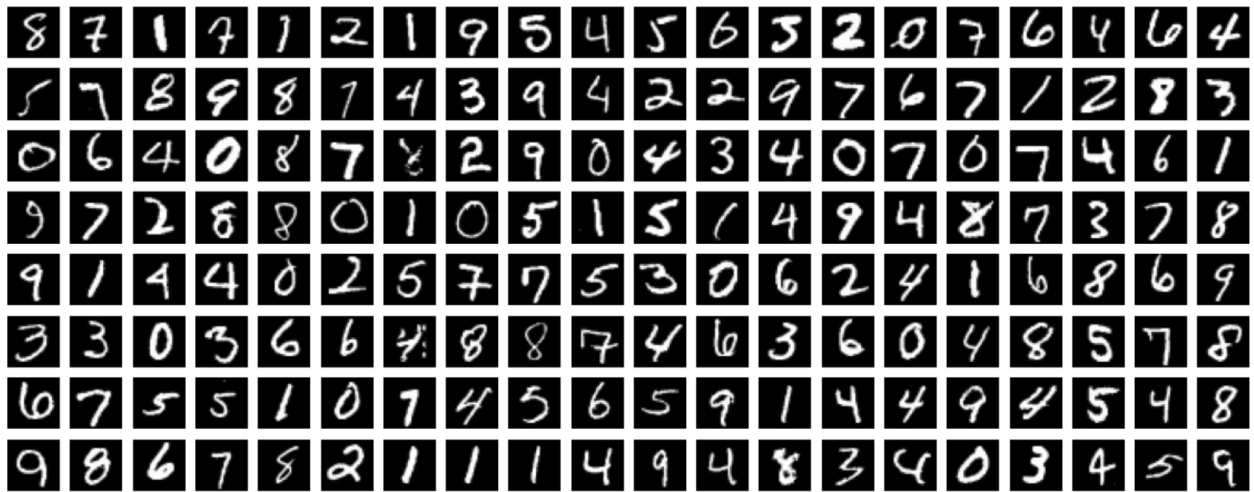


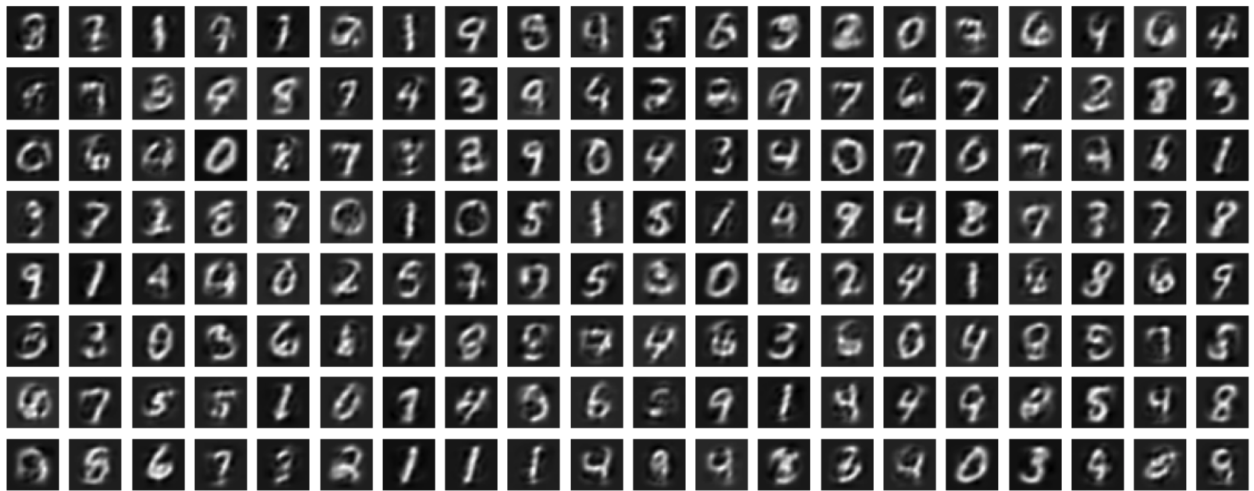
Figure 33: Reconstruction and classification results vs. the number of selected features on MNIST and MNIST-Fashion.

16 Comparisons of the reconstruction by FAE, DFAE, and CFAE

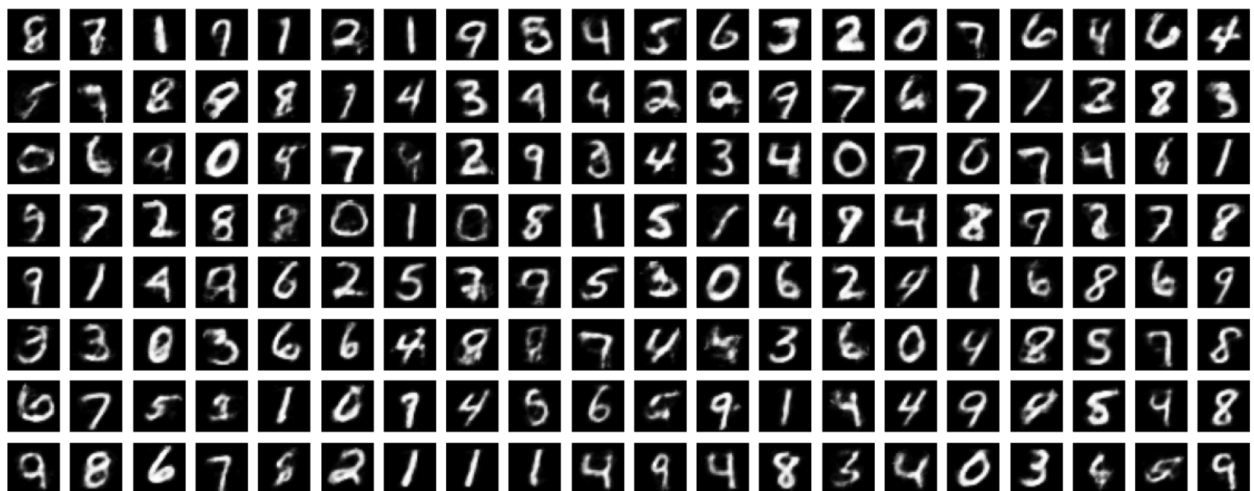
For 36 selected features, we compare the reconstruction by using FAE, DFAE, and CFAE. For illustration, here we show the reconstruction results on MNIST and MNIST-Fashion in the following Figures 34 and 35, respectively.



(a) Original testing samples



(b) Reconstruction by FAE



(c) Reconstruction by DFAE

Figure 34: Reconstruction by FAE and DFAE on MNIST.



(a) Original testing samples



(b) Reconstruction by FAE



(c) Reconstruction by CFAE

Figure 35: Reconstruction by FAE and CFAE on MNIST-Fashion.